Spontaneous emission from a dielectric slab

H. P. Urbach and G. L. J. A. Rikken*
Philips Research Laboratories, Professor Holstlaan 4, 5656 AA Eindhoven, The Netherlands
(Received 9 September 1997)

The electromagnetic field in a dielectric slab bounded by two dielectric half spaces with arbitrary refractive indices is quantized by computing the complete set of orthonormal electromagnetic modes. The zero-point fluctuations of the electromagnetic field are determined as a function of position. The dependence of the rate of spontaneous emission of thin dielectric films on the thicknesses of the films and the refractive index of the substrate is studied and compared with experimental results. [S1050-2947(98)01505-4]

PACS number(s): 42.50.Ct, 32.80.−t, 03.70.+k

I. INTRODUCTION

The atomic spontaneous emission rate can be expressed in terms of the zero-point fluctuations of the electromagnetic field at the position of the atom. The local zero-point field fluctuations depend on the photon density of states and on the electromagnetic field strengths of the modes. Because the electromagnetic fields of the modes depend strongly on the configuration and on the electromagnetic properties of the materials, the spontaneous emission rate can be either increased or decreased, depending on the electric and magnetic properties of the atom's environment.

The possibility of modifying the spontaneous emission rate by changing the environment was first pointed out by Purcell [1] in 1946. Since then experimental verifications under various conditions have been published. When free atoms are placed inside a cavity the spontaneous emission rate has been demonstrated to differ from the value in free space [2–4]. This has also been verified experimentally for certain condensed phase systems inside a cavity [5–8]. Spontaneous emission near a dielectric interface has been studied experimentally [9–11] and theoretically [12,13] and good agreement between calculations and measurements was obtained. Snoeks *et al.* [14] measured the radiative transition rate at 1.54 μm of erbium ions implanted in a thick glass layer covered by a range of transparent liquids. Rigorous computations showed that the effect of the liquid on the emission rate of Er^{3+} is fully described by the zero-point field fluctuations as a function of the distance to the interface. In [15] Yablonovitch *et al.* studied the spontaneous emission due to the recombination of electron-hole pairs in the more complicated configuration of a GaAs slab bounded by two dielectrics of lower refractive indices.

In [16] the emission rate was measured of a Eu^{3+} complex inside thin dielectric films of various thicknesses, which were spin coated onto substrates of different refractive indices. The region above the slab was in air. In order to be able to observe the change in the spontaneous emission rate, a decay process dominated by radiative decay is preferred, i.e., the luminescence quantum efficiency should be high. Furthermore, the excitation should be localized so that the change in the environment only affects the luminescence through the change in the photon modes. The required localization can be realized by using organic molecules or rare-earth ions as luminescent species. In [16] the Eu^{3+} ion was chosen as the luminescent species because of the long lifetime of the emission under certain conditions [17]. In toluene a lifetime of 0.730 ms and a quantum yield of more than 95% was observed upon excitation at 351 nm and emission at 611 nm. The transition corresponding to this emission is electric dipole allowed.

In this paper we will apply quantum electrodynamics to calculate the zero-point fluctuations of the electromagnetic field and the spontaneous emission rate from a nonabsorbing dielectric film bounded by two nonabsorbing dielectric half spaces of arbitrary refractive indices. The model will be applied to the electron-hole recombination in GaAs slabs studied in [15] and to experiments in [16] for the Eu^{3+} complex. Because in those experiments the films are thin and the substrates thick, the configuration is that of a dielectric slab bounded by two halfspaces filled with a dielectric and with air, respectively. The quantization of the electromagnetic field requires that the complete set of spatial electromagnetic modes that exist in the configuration is determined. These modes must be orthonormalized with respect to the scalar product corresponding to the electromagnetic energy density. For the dielectric film the set of modes is well known [20]. It consists of radiation modes pertaining to plane waves that are incident from either dielectric half space for both orthogonal polarizations. In addition, guided modes of either polarization may exist. These modes are evanescent in both dielectric half spaces. The claim of Yablonovitch *et al.* [15] that the guided modes do not affect the spontaneous emission rate of the electron-hole recombination due to reabsorption does not apply to the experiment of the Eu^{3+} complex because the absorption of the emitted luminescence is negligible. In fact it is found that when guided modes exist they contribute considerably to the spontaneous emission of the Eu^{3+} complex. We will list the radiation and guided modes in Secs. III and IV, respectively. The electromagnetic field will be quantized in Sec. V. In Sec. VI formulas for the spontaneous emission rate and the zero-point field fluctuations will be derived. In Sec. VII the spatial dependence of the field fluctuations will be examined and compared with results previously published by Khosravi and Loudon [18]

*Present address: Max-Planck-Institut für Festkörperforschung, Grenoble High Magnetic Field Laboratory, B.P. 166, F-38042 Grenoble Cedex 9, France.

for a symmetric configuration. Our results for this special case agree with those in that paper provided that there are no guided modes. However, when guided modes exist, our results are different due to the fact that the normalization and the density of the guided modes were not correctly computed in [18].

In Sec. VIII we will compare computed and measured spontaneous emission rates for several films and for several refractive indices of the substrate. It should be mentioned that local-field effects on a molecular scale may be very important in determining the spontaneous emission rate [19]. But since we are only interested in the emission rate of the film relative to the bulk value, the spatial electromagnetic modes do not have to be corrected for local field effects.

Some of the substrates for which the decay rate of the Eu^{3+} complex was measured have non-negligible absorption at the emission wavelength of 611 nm. The influence of the absorption in the substrate on the emission rate is most profound for the thinnest films, causing large differences between theoretical and measured rates. The model used in this paper does not apply to absorbing dielectrics. Absorption can only be incorporated by introducing the medium explicitly in a microscopic model in which a reservoir modeled by a continuum of harmonic oscillators is added to the Hamiltonian. The term of the Hamiltonian that couples the electromagnetic field and the reservoir represents the damping of the polarization. Field quantization in a homogeneous dielectric based on a microscopical model of Hopfield [21] is considered in [22,23]. The spontaneous emission in an infinite absorbing dielectric medium was shown to be modified only by the real part of the refractive index. Recently, Yeung and Gustafson [24] computed the lifetime of an excited atom near an absorbing dielectric surface using the microscopic model. The computation of the spontaneous emission for an atom in a dielectric slab will be even more complex than the computation in [24] and we will therefore not attempt to model absorption in this paper. It would, however, be interesting to check whether the microscopic Hamiltonian model correctly predicts the measured lifetimes for the dielectric film with absorbing substrates.

II. NOTATIONS

Consider an electromagnetic plane wave in a medium that is translation invariant in the x and y directions of a Cartesian coordinate system (x,y,z). Let the medium have a constant real refractive index n. The time dependence of time harmonic fields will be given by the factor $\exp(-i\omega t)$, where $\omega>0$ is the frequency. This factor will usually be omitted from the formulas. Let $\mathbf{k}=(k_x,k_y,k_z)$ be the wave vector of the plane wave so that

$$k_x^2+k_y^2+k_z^2=k^2n^2, \tag{2.1}$$

where $k=\omega(\epsilon_0\mu_0)^{1/2}$ is the wave number in vacuum. The components k_x and k_y are assumed real but $k_z=(k^2n^2-k_x^2-k_y^2)^{1/2}$ is purely imaginary when $k_x^2+k_y^2>k^2n^2$. We choose the branch of the complex square root such that the cut is along the negative real axis and such that when a is positive $a^{1/2}$ is positive and $(-a)^{1/2}=+ia^{1/2}$. Hence k_z is positive imaginary when $k_x^2+k_y^2>k^2n^2$ and the wave is then evanescent in the z direction. The plane wave can be written in a unique way as a linear combination of two orthogonally polarized plane waves, namely, a TE- or S-polarized wave, whose electric field vector is parallel to the (x,y) plane, and a TM- or P-polarized plane wave for which the magnetic field vector is parallel to this plane. It will be convenient to introduce the following two unit vectors corresponding to the electric field vector of the two polarizations:

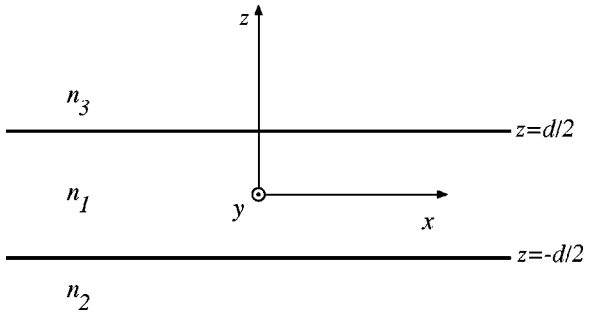

FIG. 1. Dielectric slab of a thickness d and Cartesian coordinate system (x,y,z).

$$\hat{\mathbf{i}}(\mathbf{k},S)=\frac{1}{(k_x^2+k_y^2)^{1/2}}\begin{pmatrix}k_y\\-k_x\\0\end{pmatrix}, \tag{2.2}$$

$$\hat{\mathbf{i}}(\mathbf{k},P)=\frac{1}{(k_x^2+k_y^2+|k_z|^2)^{1/2}(k_x^2+k_y^2)^{1/2}}\begin{pmatrix}k_xk_z\\k_yk_z\\-(k_x^2+k_y^2)\end{pmatrix}. \tag{2.3}$$

We have

$$\hat{\mathbf{i}}(\mathbf{k},S)\cdot\hat{\mathbf{i}}(\mathbf{k},S)^*=1,\quad \hat{\mathbf{i}}(\mathbf{k},P)\cdot\hat{\mathbf{i}}(\mathbf{k},P)^*=1, \tag{2.4}$$

$$\hat{\mathbf{i}}(\mathbf{k},S)\cdot\hat{\mathbf{i}}(\mathbf{k},P)=0,\quad \hat{\mathbf{i}}(\mathbf{k},S)\cdot\hat{\mathbf{i}}(\mathbf{k},P)^*=0, \tag{2.5}$$

where the asterisk denotes complex conjugation. Then an S-polarized plane wave is given by

$$\mathbf{E}(\mathbf{r})=A\ \exp(i\mathbf{k}\cdot\mathbf{r})\hat{\mathbf{i}}(\mathbf{k},S), \tag{2.6}$$

$$\mathbf{H}(\mathbf{r})=A(\epsilon_0/\mu_0)^{1/2}\frac{(|k_z|^2+k_x^2+k_y^2)^{1/2}}{k}\exp(i\mathbf{k}\cdot\mathbf{r})\hat{\mathbf{i}}(\mathbf{k},P), \tag{2.7}$$

where A is the amplitude of the electric field strength. Similarly, for TM- or P-polarized waves we have

$$\mathbf{E}(\mathbf{r})=A\ \exp(i\mathbf{k}\cdot\mathbf{r})\hat{\mathbf{i}}(\mathbf{k},P), \tag{2.8}$$

$$\mathbf{H}(\mathbf{r})=-A(\epsilon_0/\mu_0)^{1/2}\frac{kn^2}{(|k_z|^2+k_x^2+k_y^2)^{1/2}}\exp(i\mathbf{k}\cdot\mathbf{r})\hat{\mathbf{i}}(\mathbf{k},S). \tag{2.9}$$

Figure 1 shows the configuration that we will study in this paper. A dielectric film of thickness d and of real refractive index n_1 is bounded by two dielectric half spaces of real refractive indices n_2 and n_3. The electric permittivities of the dielectrics are ϵ_1, ϵ_2, and ϵ_3; all materials are nonmagnetic. The Cartesian coordinate system (x,y,z) is chosen

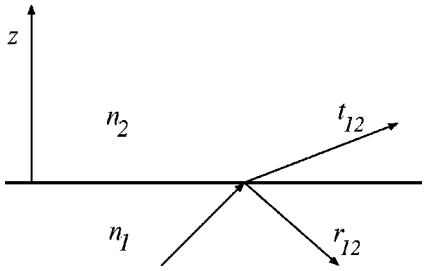

FIG. 2. Illustration of the definition of the reflection and transmission coefficients r_{12} and t_{12}.

with its origin in the middle plane of the film and with the z axis perpendicular to the interfaces. For given real k_x and k_y we will use the notation

$$k_{jz} \equiv (k^2 n_j^2 - k_x^2 - k_y^2)^{1/2} \quad \text{for } j = 1,2,3, \tag{2.10}$$

where the branch of the square root is again as described above. Furthermore, $\mathbf{k}_j^+$ and $\mathbf{k}_j^-$ are the wave vectors given by

$$\mathbf{k}_j^+ = (k_x, k_y, k_{jz}), \quad \mathbf{k}_j^- = (k_x, k_y, -k_{jz}). \tag{2.11}$$

Because of the convention that the time dependence of the fields is assumed to be given by $\exp(-i\omega t)$, it follows that when k_{jz} is real, $\mathbf{k}_j^+$ and $\mathbf{k}_j^-$ are wave vectors of plane waves that propagate in the positive and the negative z directions, respectively. When k_{jz} is imaginary, these plane waves decrease exponentially in the positive and negative z directions, respectively.

Finally, we recall that for a plane wave impinging on the interface between two dielectrics with refractive indices n_1 and n_2 incident from dielectric 1 as shown in Fig. 2, the reflection and transmission coefficients are given by

$$r_{12} = \frac{k_{1z} - k_{2z}}{k_{1z} + k_{2z}},$$

$$t_{12} = 1 + r_{12} = \frac{2k_{1z}}{k_{1z} + k_{2z}} \quad \text{for } S \text{ polarization}, \tag{2.12}$$

and

$$r_{12} = \frac{k_{1z}/n_1^2 - k_{2z}/n_2^2}{k_{1z}/n_1^2 + k_{2z}/n_2^2},$$

$$t_{12} = 1 + r_{12} = \frac{2k_{1z}/n_1^2}{k_{1z}/n_1^2 + k_{2z}/n_2^2} \quad \text{for } P \text{ polarization}. \tag{2.13}$$

III. RADIATION MODES

We will first describe the radiation modes that can exist in the configuration of Fig. 1. We distinguish between modes that are incident from medium 2 and modes that are incident from medium 3 and between S and P polarizations.

A. Modes incident from medium 2

For every frequency ω and every k_x, k_y satisfying

$$k_x^2 + k_y^2 < k^2 n_2^2, \tag{3.1}$$

where $k = \omega(\epsilon_0 \mu_0)^{1/2}$, there are S- and P-polarized electromagnetic fields in the structure consisting of plane waves and standing waves of which k_x and k_y are the components of the wave vectors in the x and y directions. The electric field of the S-polarized mode is given by

$$\mathbf{E}(\mathbf{r}) = \begin{cases} AT \exp(i\mathbf{k}_3^+ \cdot \mathbf{r}) \hat{\mathbf{i}}(\mathbf{k}_3^+, S) & \text{for } z \geq d/2, \quad (3.2a) \\ A[U \exp(i\mathbf{k}_1^+ \cdot \mathbf{r}) \hat{\mathbf{i}}(\mathbf{k}_1^+, S) + V \exp(i\mathbf{k}_1^- \cdot \mathbf{r}) \hat{\mathbf{i}}(\mathbf{k}_1^-, S)] & \text{for } -d/2 \leq z \leq d/2, \quad (3.2b) \\ A[\exp(i\mathbf{k}_2^+ \cdot \mathbf{r}) \hat{\mathbf{i}}(\mathbf{k}_2^+, S) + R \exp(i\mathbf{k}_2^- \cdot \mathbf{r}) \hat{\mathbf{i}}(\mathbf{k}_2^-, S)] & \text{for } z \leq -d/2, \quad (3.2c) \end{cases}$$

where

$$U = \frac{t_{21} \exp[i(k_{1z} - k_{2z})d/2]}{1 - r_{12} r_{13} \exp[2ik_{1z}d]}, \tag{3.3}$$

$$V = \frac{t_{21} r_{13} \exp[i(3k_{1z} - k_{2z})d/2)]}{1 - r_{12} r_{13} \exp[2ik_{1z}d]}, \tag{3.4}$$

$$T = \frac{t_{13} t_{21} \exp[i(2k_{1z} - k_{2z} - k_{3z})d/2]}{1 - r_{12} r_{13} \exp[2ik_{1z}d]}, \tag{3.5}$$

$$R = \frac{r_{21} + r_{13} \exp(2ik_{1z}d)}{1 - r_{12} r_{13} \exp[2ik_{1z}d]} \exp(-ik_{2z}d), \tag{3.6}$$

with the reflection and transmission coefficients defined by Eq. (2.12). Note that when $n_1 < n_2$ or $n_3 < n_2$, the field can depend exponentially on z in medium 1 or medium 3, respectively. When the factor A is chosen such that

$$A = \frac{1}{(2\pi)^{3/2}} \left(\frac{k}{k_{2z}} \right)^{1/2}, \tag{3.7}$$

it follows that for every $\tilde{k}$, $\tilde{k}_x$, and $\tilde{k}_y$ satisfying Eq. (3.1), with $\tilde{\mathbf{E}}$ being the electric field of the corresponding S-polarized mode, we have

$$\int\int\int \frac{\epsilon}{\epsilon_0} \mathbf{E} \cdot \tilde{\mathbf{E}}^* d\mathbf{r} = \delta(k_x - \tilde{k}_x) \delta(k_y - \tilde{k}_y) \delta(k - \tilde{k}), \tag{3.8}$$

where ϵ denotes the piecewise constant function, which is equal to ϵ_j in medium j and where δ is Dirac's delta func-

tion. All radiation modes will be parametrized by the triple k_x, k_y, k. Using Maxwell's equations and a partial integration, it is easy to verify that Eq. (3.8) implies

$$\int\int\int \frac{\mu_0}{\epsilon_0}\mathbf{H}\cdot\tilde{\mathbf{H}}^* d\mathbf{r} = \delta(k_x-\tilde{k}_x)\,\delta(k_y-\tilde{k}_y)\,\delta(k-\tilde{k}), \tag{3.9}$$

so that the modes corresponding to k, k_x, k_y and to $\tilde{k}, \tilde{k}_x, \tilde{k}_y$ are orthonormal with respect to the scalar product corresponding to the electromagnetic energy density:

$$\frac{1}{2}\int\int\int\left[\frac{\epsilon}{\epsilon_0}\mathbf{E}\cdot\tilde{\mathbf{E}}^* + \frac{\mu_0}{\epsilon_0}\mathbf{H}\cdot\tilde{\mathbf{H}}^*\right]d\mathbf{r} = \delta(k_x-\tilde{k}_x)\,\delta(k_y-\tilde{k}_y)\,\delta(k-\tilde{k}). \tag{3.10}$$

The statement that the orthonormality relation for the electric field (3.8) implies the orthonormality condition (3.10) for the electromagnetic field in fact applies to all modes in the slab geometry and we will subsequently disregard the magnetic field and give the relevant expressions for the electric field only.

The electric field of the P-polarized mode corresponding to k_x, k_y, and k that satisfy Eq. (3.1) is given by

$$\mathbf{E}(\mathbf{r}) = \begin{cases} A\dfrac{n_2(k_x^2+k_y^2+|k_{3z}|^2)^{1/2}}{n_3^2 k}\,T\,\exp(i\mathbf{k}_3^+\cdot\mathbf{r})\hat{\mathbf{i}}(\mathbf{k}_3^+,P) & \text{for } z\geqslant d/2, \quad (3.11a)\\ A\dfrac{n_2(k_x^2+k_y^2+|k_{1z}|^2)^{1/2}}{n_1^2 k}[U\,\exp(i\mathbf{k}_1^+\cdot\mathbf{r})\hat{\mathbf{i}}(\mathbf{k}_1^+,P)+V\,\exp(i\mathbf{k}_1^-\cdot\mathbf{r})\hat{\mathbf{i}}(\mathbf{k}_1^-,P)] & \text{for } -d/2\leqslant z\leqslant d/2, \quad (3.11b)\\ A[\exp(i\mathbf{k}_2^+\cdot\mathbf{r})\hat{\mathbf{i}}(\mathbf{k}_2^+,P)+R\,\exp(i\mathbf{k}_2^-\cdot\mathbf{r})\hat{\mathbf{i}}(\mathbf{k}_2^-,P)] & \text{for } z\leqslant -d/2, \quad (3.11c)\end{cases}$$

where U, V, T, and R are again given by Eqs. (3.3), (3.4), (3.5), and (3.6), but now the reflection and transmission coefficients are those for P-polarized plane waves, i.e., they are given by (2.13). The choice (3.7) for A again leads to orthonormality relation (3.8) for the electric fields of two P-polarized modes. Orthonormality relation (3.10) for the total electromagnetic fields is then also satisfied. Furthermore, S-polarized and P-polarized modes are always orthogonal.

B. Modes incident from medium 3

For all values of k, k_x, and k_y satisfying

$$k_x^2+k_y^2<k^2n_3^2, \tag{3.12}$$

there are S- and P-polarized electromagnetic fields that are incident from medium 3 and consist of plane waves and standing waves of which k_x and k_y are the components of the wave vectors in the x and y directions. The electric fields are obtained by interchanging media 2 and 3 and the superscripts + and − in the expressions (3.2a), (3.2b), (3.2c) and (3.11a), (3.11b), (3.11c). Hence, for S polarization the electric field is given by

$$\mathbf{E}(\mathbf{r}) = \begin{cases} A[\exp(i\mathbf{k}_3^-\cdot\mathbf{r})\hat{\mathbf{i}}(\mathbf{k}_3^-,S)+R\,\exp(i\mathbf{k}_3^+\cdot\mathbf{r})\hat{\mathbf{i}}(\mathbf{k}_3^+,S)] & \text{for } z\geqslant d/2, \quad (3.13a)\\ A[U\,\exp(i\mathbf{k}_1^-\cdot\mathbf{r})\hat{\mathbf{i}}(\mathbf{k}_1^-,S)+V\,\exp(i\mathbf{k}_1^+\cdot\mathbf{r})\hat{\mathbf{i}}(\mathbf{k}_1^+,S)] & \text{for } -d/2\leqslant z\leqslant d/2, \quad (3.13b)\\ AT\,\exp(i\mathbf{k}_2^-\cdot\mathbf{r})\hat{\mathbf{i}}(\mathbf{k}_2^-,S) & \text{for } z\leqslant -d/2, \quad (3.13c)\end{cases}$$

where

$$U = \frac{t_{31}\exp[i(k_{1z}-k_{3z})d/2]}{1-r_{13}r_{12}\exp[2ik_{1z}d]}, \tag{3.14}$$

$$V = \frac{t_{31}r_{12}\exp[i(3k_{1z}-k_{3z})d/2)]}{1-r_{13}r_{12}\exp[2ik_{1z}d]}, \tag{3.15}$$

$$T = \frac{t_{12}t_{31}\exp[i(2k_{1z}-k_{3z}-k_{2z})d/2]}{1-r_{13}r_{12}\exp[2ik_{1z}d]}, \tag{3.16}$$

$$R = \frac{r_{31}+r_{12}\exp(2ik_{1z}d)}{1-r_{13}r_{12}\exp[2ik_{1z}d]}\exp(-ik_{3z}d), \tag{3.17}$$

with the reflection and transmission coefficients given by Eq. (2.12). When

$$A = \frac{1}{(2\pi)^{3/2}}\left(\frac{k}{k_{3z}}\right)^{1/2}, \tag{3.18}$$

the electric fields are orthonormal in the sense of Eq. (3.8).

By analogy, for P-polarized modes that are incident from medium 3 the electric field is

$$\mathbf{E}(\mathbf{r})=\begin{cases} A[\exp(i\mathbf{k}_3^-\cdot\mathbf{r})\hat{\mathbf{i}}(\mathbf{k}_3^-,P)+R\ \exp(i\mathbf{k}_3^+\cdot\mathbf{r})\hat{\mathbf{i}}(\mathbf{k}_3^+,P)] & \text{for } z\geqslant d/2, \quad (3.19a)\\ A\dfrac{n_3(k_x^2+k_y^2+|k_{1z}|^2)^{1/2}}{n_1^2k}[U\ \exp(i\mathbf{k}_1^-\cdot\mathbf{r})\hat{\mathbf{i}}(\mathbf{k}_1^-,P)+V\ \exp(i\mathbf{k}_1^+\cdot\mathbf{r})\hat{\mathbf{i}}(\mathbf{k}_1^+,P)] & \text{for } -d/2\leqslant z\leqslant d/2, \quad (3.19b)\\ A\dfrac{n_3(k_x^2+k_y^2+|k_{2z}|^2)^{1/2}}{n_2^2k}T\ \exp(i\mathbf{k}_2^-\cdot\mathbf{r})\hat{\mathbf{i}}(\mathbf{k}_2^-,P) & \text{for } z\leqslant -d/2, \quad (3.19c)\end{cases}$$

where U, V, T, and R are again defined by Eqs. (3.14), (3.15), (3.16), and (3.17) but with the reflection and transmission coefficients now being given by Eq. (2.13). When A satisfies Eq. (3.18) the electric fields again satisfy orthonormality relation (3.8). Furthermore, S-polarized and P-polarized modes are orthogonal.

It is not difficult to see that two radiation modes, one being incident from medium 2 and the other from medium 3, are orthogonal in the sense of Eq. (3.8), i.e., when $\mathbf{E}$ and $\tilde{\mathbf{E}}$ are the corresponding electric fields, then

$$\int\int\int \frac{\epsilon}{\epsilon_0}\mathbf{E}\cdot\tilde{\mathbf{E}}^*d\mathbf{r}=0. \quad (3.20)$$

This is also true when $\tilde{k}_x=k_x$, $\tilde{k}_y=k_y$, and $\tilde{k}=k$ and the polarizations are the same. As remarked above, Eq. (3.20) implies that not only the electric fields but also the magnetic fields are orthogonal with respect to the scalar product (3.9).

IV. GUIDED MODES

Guided modes may exist when

$$\max(n_2,n_3)<n_1. \quad (4.1)$$

This condition is always necessary for the existence of guided modes but it is sufficient only when $n_2=n_3$ [20]. Guided modes are evanescent in both half spaces. Hence both k_{2z} and k_{3z} must be purely imaginary and therefore $(k_x^2+k_y^2)^{1/2}>k\ \max(n_2,n_3)$. It is easy to see that when $(k_x^2+k_y^2)^{1/2}\geqslant kn_1$ modes cannot exist. Hence for guided modes the following inequalities are satisfied:

$$k\ \max(n_2,n_3)<(k_x^2+k_y^2)^{1/2}<kn_1. \quad (4.2)$$

The length of the projection of the wave vector on the (x,y) plane, $\beta\equiv(k_x^2+k_y^2)^{1/2}$, is called the propagation constant of the guided mode. For a given value of the wave number k in vacuum, or equivalently for a given frequency ω, there is at most a finite number of propagation constants in the interval defined by Eq. (4.2). The set of β's is different for the two polarizations. We will consider S and P polarization separately.

A. S-polarized guided modes

The equation to be satisfied by the propagation constant β of S-polarized guided modes is [20]

$$r_{12}r_{13}\exp(2ik_{1z}d)=1, \quad (4.3)$$

or, using Eq. (2.12),

$$\tan(k_{1z}d)=\frac{k_{1z}(|k_{2z}|+|k_{3z}|)}{k_{1z}^2-|k_{2z}||k_{3z}|}. \quad (4.4)$$

When $n_1>n_2\geqslant n_3$ the number M_S of propagation constants of S-polarized guided modes is given by

$$M_S=\max\left(0,1+\left[\frac{kd}{\pi}(n_1^2-n_2^2)^{1/2}-\frac{1}{\pi}\arctan\left\{\left(\frac{n_2^2-n_3^2}{n_1^2-n_2^2}\right)^{1/2}\right\}\right]\right), \quad (4.5)$$

where $[\xi]$ denotes the largest integer that is smaller than or equal to ξ. It follows from Eq. (4.5) that when $n_2=n_3$ we have $M_S\geqslant 1$ so that in that case there is at least one propagation constant corresponding to S-polarized guided modes. When $n_1>n_3>n_2$, the number of propagation constants of S-polarized guided modes is again given by Eq. (4.5) but with n_2 and n_3 interchanged.

The propagation constants are ordered so that

$$k\ \max(n_2,n_3)<\beta_{M_S}<\cdots<\beta_1<kn_1. \quad (4.6)$$

When for certain values of the wave number k, the thickness of the film and the refractive indices the lowest propagation constant β_{M_S} converges to the lower bound $k\ \max(n_2,n_3)$, then in this limit the lowest guided mode is said to be at the cutoff and the number M_S of S-polarized guided modes is decreased by 1.

The electric field of an S-polarized guided mode is given by

$$\mathbf{E}(\mathbf{r})=\begin{cases} AT_3\exp(i\mathbf{k}_3^+\cdot\mathbf{r})\hat{\mathbf{i}}(\mathbf{k}_3^+,S) & \text{for } z\geqslant d/2, \quad (4.7a)\\ A[\exp(i\mathbf{k}_1^+\cdot\mathbf{r})\hat{\mathbf{i}}(\mathbf{k}_1^+,S)+V\exp(i\mathbf{k}_1^-\cdot\mathbf{r})\hat{\mathbf{i}}(\mathbf{k}_1^-,S)] & \text{for } -d/2\leqslant z\leqslant d/2, \quad (4.7b)\\ AT_2\exp(i\mathbf{k}_2^-\cdot\mathbf{r})\hat{\mathbf{i}}(\mathbf{k}_2^-,S) & \text{for } z\leqslant -d/2, \quad (4.7c)\end{cases}$$

where

$$T_3=t_{13}\exp[i(k_{1z}-k_{3z})d/2], \quad (4.8)$$

$$V=r_{13}\exp(ik_{1z}d), \quad (4.9)$$

$$T_2=\frac{t_{12}}{r_{12}}\exp[-i(k_{1z}+k_{2z})d/2]. \quad (4.10)$$

The reflection and transmission coefficients are of course those for S-polarized fields.

When the half spaces consist of the same media we have $n_3=n_2$ and hence Eq. (4.3) becomes $r_{12}^2\exp(2ik_{1z}d)=1$. The electric fields of the guided modes are then symmetric or antisymmetric functions of z depending on whether the propagation constant satisfies $r_{12}\exp(ik_{1z}d)=+1$ or $r_{12}\exp(ik_{1z}d)=-1$, respectively.

When

$$A=\frac{1}{2\pi\sqrt{2}}\left[n_1^2d+\frac{n_1^2}{k_{1z}}\frac{k_{1z}^2+|k_{2z}k_{3z}|}{k_{1z}^2-|k_{2z}k_{3z}|}\cos(k_{1z}d)\sin(k_{1z}d)+\frac{n_2^2}{|k_{2z}|}\frac{k_{1z}^2}{k_{1z}^2+|k_{2z}|^2}+\frac{n_3^2}{|k_{3z}|}\frac{k_{1z}^2}{k_{1z}^2+|k_{3z}|^2}\right]^{-1/2} \quad (4.11)$$

is chosen, the electric fields become normalized in the sense that for two S-polarized guided modes corresponding to k_x, k_y, ν and $\tilde{k}_x$, $\tilde{k}_y$, $\tilde{\nu}$ with electric fields $\mathbf{E}$ and $\tilde{\mathbf{E}}$, respectively, we have

$$\int\int\int \frac{\epsilon}{\epsilon_0}\mathbf{E}\cdot\tilde{\mathbf{E}}^*d\mathbf{r}=\delta(k_x-\tilde{k}_x)\delta(k_y-\tilde{k}_y)\delta_{\nu\tilde{\nu}}, \quad (4.12)$$

where $\delta_{\nu\tilde{\nu}}=1$ if $\nu=\tilde{\nu}$ and $=0$ otherwise.

Let the thickness d of the film and the refractive indices n_1, n_2, and n_3 all be fixed. We regard the wave number k in vacuum as a variable. Equation (4.4) has for every value of k finitely many solutions for the propagation constant and we will regard these solutions as functions of k: $\beta_\nu^S(k)$, $\nu=1,\ldots,M_S$. Note that M_S depends on k. The superscript S is now added to β to emphasize the polarization dependence of the propagation constants. It follows from Eq. (4.2) that

$$k\ \max(n_2,n_3)<\beta_\nu^S(k)<kn_1. \quad (4.13)$$

When $\beta_\nu^S(k)$ reaches the lower bound, guided mode ν is cut off. Furthermore, $\beta_\nu^S(k)$ is an increasing function of k. Let $k_\nu^S(\beta)$ be the inverse of $\beta_\nu^S(k)$. Four of these functions are shown in Fig. 3 for certain values of n_1, n_2, and n_3. In the three-dimensional parameter space (k_x,k_y,k), the total set of S-polarized guided modes consists of disjunct surfaces obtained by rotating the curves shown in Fig. 3 around the k axis. These surfaces are conveniently parametrized by k_x and k_y:

$$k=k_\nu^S(\sqrt{k_x^2+k_y^2}), \quad (4.14)$$

where $\sqrt{k_x^2+k_y^2}>\beta_\nu^{S,\min}$ with $\beta=\beta_\nu^{S,\min}$ satisfying

$$\beta=k_\nu^S(\beta)\max(n_2,n_3). \quad (4.15)$$

To $\beta_\nu^{S,\min}$ corresponds $k_\nu^{S,\min}$ defined by

$$k_\nu^{S,\min}=k_\nu^S(\beta_\nu^{S,\min}), \quad (4.16)$$

The S-polarized νth guided mode exists only when $\beta>\beta_\nu^{S,\min}$, or equivalently when $k>k_\nu^{S,\min}$.

B. *P*-polarized guided modes

The equation for the propagation constant β of P-polarized guided modes is again given by Eq. (4.3), but now the reflection coefficients are those for the P-polarized case. Substitution of Eq. (2.13) into (4.3) yields

$$\tan(k_{1z}d)=\frac{(k_{1z}/n_1^2)(|k_{2z}|/n_2^2+|k_{3z}|/n_3^2)}{k_{1z}^2/n_1^4-|k_{2z}||k_{3z}|/n_2^2n_3^2}. \quad (4.17)$$

When $n_1>n_2\geqslant n_3$, the number M_P of propagation constants of P-polarized guided modes is given by

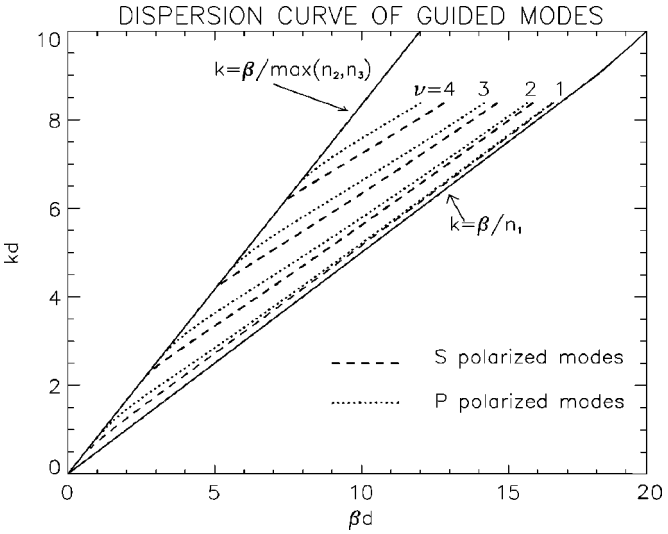

FIG. 3. The curves $k=k_\nu^S(\beta)$ and $k=k_\nu^P(\beta)$ for $\nu=1,2,3,4$, corresponding to the S-polarized and the P-polarized guided modes of a slab with refractive indices $n_1=2.0$, $n_2=1.2$, and $n_3=1.0$.

$$M_P=\max\left(0,1+\left[\frac{kd}{\pi}(n_1^2-n_2^2)^{1/2}-\frac{1}{\pi}\arctan\left\{\frac{n_1^2}{n_3^2}\left(\frac{n_2^2-n_3^2}{n_1^2-n_2^2}\right)^{1/2}\right\}\right]\right), \tag{4.18}$$

where the square brackets have the same meaning as in Eq. (4.5). The number M_P is smaller than or equal to the number M_S for S polarization. It is seen that when $n_2=n_3$ we have $M_P\geqslant 1$, and since also $M_S\geqslant 1$ in this case, it follows that the symmetric slab waveguide has at least two propagation constants, one corresponding to an S-polarized and the other to a P-polarized guided mode. When $n_1>n_3>n_2$, the number of propagation constants of P-polarized guided modes is again given by Eq. (4.18) but with n_2 and n_3 interchanged. The propagation constants of the P-polarized mode are ordered as in Eq. (4.6).

The electric field of a P-polarized guided mode is

$$\mathbf{E}(\mathbf{r})=\begin{cases} A\dfrac{n_1(k_x^2+k_y^2+|k_{3z}|^2)^{1/2}}{n_3^2k}T_3\exp(i\mathbf{k}_3^+\cdot\mathbf{r})\hat{\mathbf{i}}(\mathbf{k}_3^+,P) & \text{for } z\geqslant d/2, \quad (4.19a)\\ A[\exp(i\mathbf{k}_1^+\cdot\mathbf{r})\hat{\mathbf{i}}(\mathbf{k}_1^+,P)+V\exp(i\mathbf{k}_1^-\cdot\mathbf{r})\hat{\mathbf{i}}(\mathbf{k}_1^-,P)] & \text{for } -d/2\leqslant z\leqslant d/2, \quad (4.19b)\\ A\dfrac{n_1(k_x^2+k_y^2+|k_{2z}|^2)^{1/2}}{n_2^2k}T_2\exp(i\mathbf{k}_2^-\cdot\mathbf{r})\hat{\mathbf{i}}(\mathbf{k}_2^-,P) & \text{for } z\leqslant -d/2, \quad (4.19c)\end{cases}$$

where T_3, V, and T_2 are given by Eqs. (4.8), (4.9), and (4.10), with the Fresnel coefficients being given by Eq. (2.13). When $n_2=n_3$ the electric fields of the guided modes are either symmetric or antisymmetric functions of z depending on whether $r_{12}\exp(ik_{1z}d)=+1$ or $r_{12}\exp(ik_{1z}d)=-1$, respectively.

When

$$A=\frac{1}{2\pi\sqrt{2}}\left[n_1^2d+\frac{n_1^2}{k_{1z}}\frac{k_{1z}^2/n_1^4+|k_{2z}k_{3z}|/(n_2^2n_3^2)}{k_{1z}^2/n_1^4-|k_{2z}k_{3z}|/(n_2^2n_3^2)}\cos(k_{1z}d)\sin(k_{1z}d)+\frac{k_{1z}^2/n_1^2}{|k_{2z}|(k_{1z}^2/n_1^4+|k_{2z}|^2/n_2^4)}+\frac{k_{1z}^2/n_1^2}{|k_{3z}|(k_{1z}^2/n_1^4+|k_{3z}|^2/n_3^4)}\right]^{-1/2} \tag{4.20}$$

is chosen, orthonormality condition (4.12) is satisfied. It can be shown that the electric fields (and hence also the magnetic fields) corresponding to two guided modes of different orthogonal polarizations, and the electric fields corresponding to a guided mode and a radiation mode of either polarization are orthogonal.

As in the S-polarized case, the propagation constants are regarded as functions of the wave number in vacuum k and denoted by $\beta_\nu^P(k)$. Let $k_\nu^P(\beta)$ be the inverse of $\beta_\nu^P(k)$. Four of these functions are shown in Fig. 3 for a particular slab. Then, as in the S-polarized case, the total set of P-polarized guided modes in three-dimensional (k_x,k_y,k) parameter space consists of surfaces given by

$$k=k_\nu^P(\sqrt{k_x^2+k_y^2}), \tag{4.21}$$

where $\sqrt{k_x^2+k_y^2}>\beta_\nu^{P,\min}$ with $\beta=\beta_\nu^{P,\min}$ satisfying

$$\beta=k_\nu^P(\beta)\max(n_2,n_3), \tag{4.22}$$

We define

$$k_\nu^{P,\min}=k_\nu^P(\beta_\nu^{P,\min}). \tag{4.23}$$

Then the νth P-polarized guided mode exists provided that $\beta>\beta_\nu^{P,\min}$, or equivalently that $k>k_\nu^{P,\min}$.

V. FIELD QUANTIZATION

The radiation modes are labeled by the triple $\kappa=(k_x,k_y,k)$, where $k=\omega/c$ is the wave number in vacuum, by the index λ, which specifies the polarization ($\lambda=S$ or $\lambda=P$) and by the index μ, which specifies the medium from which the radiation mode is incident (i.e., $\mu=2$ or $\mu=3$). The electric fields of the radiation modes are thus denoted by $\mathbf{E}_{\kappa\lambda\mu}$.

The guided modes are labeled by $\bar{\kappa}=(k_x,k_y)$, λ, and ν, where ν is the index of the propagation constant of the guided mode. The electric field of a guided mode is denoted by $\mathbf{E}_{\bar{\kappa}\lambda\nu}^-$.

The orthogonality relations (3.8), (4.12) for the modes can be summarized as follows:

$$\int\int\int \frac{\epsilon}{\epsilon_0}\mathbf{E}_{\kappa_1\lambda_1\mu_1}\cdot\mathbf{E}^*_{\kappa_2\lambda_2\mu_2}d\mathbf{r}=\delta(\kappa_1-\kappa_2)\,\delta_{\lambda_1\lambda_2}\delta_{\mu_1\mu_2}, \tag{5.1a}$$

$$\int\int\int \frac{\epsilon}{\epsilon_0}\mathbf{E}^-_{\bar{\kappa}_1\lambda_1\nu_1}\cdot\mathbf{E}^*_{\bar{\kappa}_2\lambda_2\nu_2}d\mathbf{r}=\delta(\bar{\kappa}_1-\bar{\kappa}_2)\,\delta_{\lambda_1\lambda_2}\delta_{\nu_1\nu_2}, \tag{5.1b}$$

$$\int\int\int \frac{\epsilon}{\epsilon_0}\mathbf{E}^-_{\bar{\kappa}_1\lambda_1\nu_1}\cdot\mathbf{E}^*_{\kappa_2\lambda_2\mu_2}d\mathbf{r}=0. \tag{5.1c}$$

The set of electromagnetic fields of the radiation and the guided modes is a complete orthonormal set of eigenfunctions of Maxwell's equations in the space of all pairs $(\mathbf{E},\mathbf{H})$ of transverse square integrable vector fields, equipped with the scalar product defined by the left-hand side of Eq. (3.10). By definition transverse fields satisfy

$$\nabla\cdot(\epsilon\mathbf{E})=\mathbf{0},\quad \nabla\cdot\mathbf{H}=\mathbf{0}. \tag{5.2}$$

A mathematical proof of the completeness has been given by Weder [25].

Let $\hat{a}_{\kappa\lambda\mu}$ and $\hat{a}^{\dagger}_{\kappa\lambda\mu}$ be the destruction and creation operators corresponding to the radiation modes and let $\hat{a}_{\overline{\kappa\lambda}\nu}$ and $\hat{a}^{\dagger}_{\overline{\kappa\lambda}\nu}$ be the corresponding operators for the guided modes. These operators satisfy the commutation relations

$$[\hat{a}_{\kappa_1\lambda_1\mu_1},\hat{a}^{\dagger}_{\kappa_2\lambda_2\mu_2}]=\delta(\kappa_1-\kappa_2)\,\delta_{\lambda_1\lambda_2}\delta_{\mu_1\mu_2}, \tag{5.3a}$$

$$[\hat{a}_{\overline{\kappa}_1\lambda_1\nu_1},\hat{a}^{\dagger}_{\overline{\kappa}_2\lambda_2\nu_2}]=\delta(\overline{\kappa}_1-\overline{\kappa}_2)\,\delta_{\lambda_1\lambda_2}\delta_{\nu_1\nu_2}, \tag{5.3b}$$

$$[\hat{a}_{\kappa_1\lambda_1\mu_1},\hat{a}_{\kappa_2\lambda_2\mu_2}]=[\hat{a}^{\dagger}_{\kappa_1\lambda_1\mu_1},\hat{a}^{\dagger}_{\kappa_2\lambda_2\mu_2}]=0, \tag{5.3c}$$

$$[\hat{a}_{\overline{\kappa}_1\lambda_1\nu_1},\hat{a}_{\overline{\kappa}_2\lambda_2\nu_2}]=[\hat{a}^{\dagger}_{\overline{\kappa}_1\lambda_1\nu_1},\hat{a}^{\dagger}_{\overline{\kappa}_2\lambda_2\nu_2}]=0, \tag{5.3d}$$

$$[\hat{a}_{\overline{\kappa}_1\lambda_1\nu_1},\hat{a}_{\kappa_2\lambda_2\mu_2}]=[\hat{a}_{\overline{\kappa}_1\lambda_1\nu_1},\hat{a}^{\dagger}_{\kappa_2\lambda_2\mu_2}]=[\hat{a}^{\dagger}_{\overline{\kappa}_1\lambda_1\nu_1},\hat{a}^{\dagger}_{\kappa_2\lambda_2\mu_2}]=0. \tag{5.3e}$$

The transverse electric field operator is

$$\hat{\mathbf{E}}(\mathbf{r},t)=\hat{\mathbf{E}}^{-}(\mathbf{r},t)+\hat{\mathbf{E}}^{+}(\mathbf{r},t), \tag{5.4}$$

where

$$\hat{\mathbf{E}}^{+}(\mathbf{r},t)=i\sum_{\lambda=S,P}\sum_{\mu=2}^{3}\int\int\int_{(k_x^2+k_y^2)^{1/2}<kn_\mu}\left(\frac{\hbar\omega}{2\epsilon_0}\right)^{1/2}\mathbf{E}_{\kappa\lambda\mu}(\mathbf{r})\exp(-i\omega t)\big|_{\omega=ck}\hat{a}_{\kappa\lambda\mu}dk_x dk_y dk$$
$$+i\sum_{\lambda=S,P}\sum_{\nu=1}^{\infty}\int\int_{\beta>\beta_\nu^{\lambda,\min}}\left(\frac{\hbar\omega}{2\epsilon_0}\right)^{1/2}\mathbf{E}^{-}_{\kappa\lambda\nu}(\mathbf{r})\exp(-i\omega t)\big|_{\omega=ck_\nu^\lambda(\beta)}\hat{a}_{\overline{\kappa\lambda}\nu}dk_x dk_y, \tag{5.5}$$

and $\hat{\mathbf{E}}^{-}(\mathbf{r},t)$ is the adjoint of $\hat{\mathbf{E}}^{+}(\mathbf{r},t)$. In the second integral to the right of Eq. (5.5) we used the notation $\beta=(k_x^2+k_y^2)^{1/2}$; the integration with respect to k_x, k_y extends over the exterior of the circle $\beta=\beta_\nu^{\lambda,\min}$ with $\beta_\nu^{\lambda,\min}$ being defined by Eqs. (4.15) and (4.22). On this circle the λ-polarized νth guided mode is cut off.

When Eqs. (5.1) and (5.3) are used it follows that the contribution of the transverse electric field operator to the Hamiltonian for the total electromagnetic field is given by

$$\frac{1}{2}\int\int\int\epsilon\hat{\mathbf{E}}(\mathbf{r},t)\cdot\hat{\mathbf{E}}(\mathbf{r},t)^{*}d\mathbf{r}=\frac{1}{2}\sum_{\lambda=S,P}\sum_{\mu=2}^{3}\int\int\int_{(k_x^2+k_y^2)^{1/2}<kn_\mu}\hbar\omega\big|_{\omega=ck}\left[\hat{a}^{\dagger}_{\kappa\lambda\mu}\hat{a}_{\kappa\lambda\mu}+\frac{1}{2}\right]dk_x dk_y dk$$
$$+\frac{1}{2}\sum_{\lambda=S,P}\sum_{\nu=1}^{\infty}\int\int_{\beta>\beta_\nu^{\lambda,\min}}\hbar\omega\big|_{\omega=ck_\nu^\lambda(\beta)}\left[\hat{a}^{\dagger}_{\overline{\kappa\lambda}\nu}\hat{a}_{\overline{\kappa\lambda}\nu}+\frac{1}{2}\right]dk_x dk_y. \tag{5.6}$$

The contribution to the Hamiltonian of the magnetic field operator is identical to that of the electric field operator. Hence the total Hamiltonian of the electromagnetic field is given by the well-known superposition of the number operators of all electromagnetic modes.

VI. SPONTANEOUS EMISSION RATE AND ZERO-POINT FIELD FLUCTUATIONS

Suppose that an atom makes a spontaneous dipole transition from a state $|2\rangle$ to a state $|1\rangle$ thereby emitting a photon of energy $\hbar\omega_0$. The spontaneous emission can occur in any mode of the electromagnetic field of frequency ω_0, or equivalently of wave number $k_0=\omega_0/c$ in vacuum. The transition rate into a particular electromagnetic mode with parameters κ,λ,μ, say, and with wave number k in vacuum, is given by [26]

$$\frac{2\pi}{c\hbar^2}|\langle f|\hat{\mathcal{H}}_{\mathrm{ED}}|i\rangle|^2\delta(k_0-k), \tag{6.1}$$

where $|i\rangle$ and $|f\rangle$ are the initial and final states of the combined atom-radiation system and $\hat{\mathcal{H}}_{\mathrm{ED}}$ is the electric-dipole interaction part of the complete Hamiltonian of the atom-radiation system. In the initial state of the electromagnetic field no photons are present. In the final state there is one photon in the mode with parameters κ,λ,μ. Because the transition rate is much smaller than the transition frequency, the Lorentzian line is extremely peaked. Hence, in a good approximation only modes of energy identical to the transition energy contribute to the transition.

According to Fermi's ''golden rule,'' the total spontaneous emission rate is obtained by integrating Eq. (6.1) over all the final states. Suppose that the dipole moment of the atom is parallel to one of the axes of the Cartesian coordinate system and let j be x, y, or z. Let $\hat{E}^j$ be the jth component of the transverse electric field operator. Then the total spontaneous emission rate of an atom at position $\mathbf{r}$ whose dipole moment is parallel to the j axis is ([18])

$$\frac{1}{\tau}=\frac{2\pi e^2}{\hbar^2 c}|\mathbf{D}_{12}|^2\mathcal{F}^j(z), \tag{6.2}$$

where e is the electron charge, $\mathbf{D}_{12}$ is the dipole matrix element of the atomic transition, and

$$\mathcal{F}^j(z)=\sum_{\lambda=S,P}\sum_{\mu=2}^{3}\int\int\int_{(k_x^2+k_y^2)^{1/2}<kn_\mu}\frac{\hbar\omega}{2\epsilon_0}|E^j_{\kappa\lambda\mu}(\mathbf{r})|^2\delta(k_0-k)dk_x dk_y dk$$
$$+\sum_{\lambda=S,P}\sum_{\nu=1}^{\infty}\int\int_{\beta>\beta_\nu^{\lambda,\min}}\frac{\hbar\omega}{2\epsilon_0}|E^j_{\bar{\kappa}\lambda\nu}(\mathbf{r})|^2\delta(k_0-k_\nu^\lambda(\beta))dk_x dk_y, \tag{6.3}$$

where in the integrand of the first term to the right $\omega=ck$ whereas in the integrand of the second term $\omega=ck_\nu^\lambda(\beta)$. The function $\mathcal{F}^j$ clearly depends only on the coordinate z and is independent of x and y. Note that without the delta function in the integrands, Eq. (6.3) is the jth component of the zero-point electromagnetic field fluctuations $\langle 0|\hat{E}^j(\mathbf{r})^2|0\rangle$. Hence $\mathcal{F}^j(z)$ is the contribution (per wave number) of all modes of wave number k_0 to the jth component of the zero-point field fluctuations. We will refer to $\mathcal{F}^j(z)$ as the jth component of the zero-point field fluctuations in the understanding that only the contributions of the modes of wave number k_0 are meant.

When polar coordinates are introduced in the (k_x,k_y) plane:

$$k_x=\beta\cos\varphi,\quad k_y=\beta\sin\varphi, \tag{6.4}$$

Eq. (6.3) becomes

$$\mathcal{F}^j(z)=\sum_{\lambda=S,P}\sum_{\mu=2}^{3}\int_0^{2\pi}\int_0^{\infty}\int_0^{kn_\mu}\frac{\hbar\omega}{2\epsilon_0}|E^j_{\kappa\lambda\mu}(\mathbf{r})|^2|_{\kappa=(\beta\cos\varphi,\beta\sin\varphi,k)}\delta(k_0-k)\beta d\beta dk d\varphi$$
$$+\sum_{\lambda=S,P}\sum_{\nu=1}^{\infty}\int_0^{2\pi}\int_{\beta_\nu^{\lambda,\min}}^{\infty}\frac{\hbar\omega}{2\epsilon_0}|E^j_{\bar{\kappa}\lambda\nu}(\mathbf{r})|^2|_{\bar{\kappa}=(\beta\cos\varphi,\beta\sin\varphi)}\delta(k_0-k_\nu^\lambda(\beta))\beta d\beta d\varphi \tag{6.5}$$

$$=\sum_{\lambda=S,P}\sum_{\mu=2}^{3}\int_0^{2\pi}\int_0^{k_0 n_\mu}\frac{\hbar\omega_0}{2\epsilon_0}|E^j_{\kappa\lambda\mu}(\mathbf{r})|^2|_{\kappa=(\beta\cos\varphi,\beta\sin\varphi,k_0)}\beta d\beta d\varphi$$
$$+\sum_{\lambda=S,P}\sum_{\substack{\nu\geq 1\\ k_\nu^{\lambda,\min}<k_0}}\int_0^{2\pi}\frac{\hbar\omega_0}{2\epsilon_0}|E^j_{\bar{\kappa}\lambda\nu}(\mathbf{r})|^2|_{\bar{\kappa}=(\beta_\nu^\lambda(k_0)\cos\varphi,\beta_\nu^\lambda(k_0)\sin\varphi)}\beta_\nu^\lambda(k_0)\frac{d\beta_\nu^\lambda}{dk}(k_0)d\varphi. \tag{6.6}$$

Note that the constraint $k_\nu^{\lambda\ \min}<k_0$ makes the last sum in Eq. (6.6) over ν finite. It should furthermore be noted that when for some ν and λ it happens that $k_0=k_\nu^\lambda(\beta_\nu^{\lambda,\min})$, the δ function $\delta(k_0-k_\nu^\lambda(\beta))$ is concentrated at the boundary of the integration interval in the inner integral of the second term to the right of Eq. (6.5). Physically this means that the λ-polarized νth guided mode is at a cut off. It can be shown that the evaluation of this inner integral is nevertheless not ambiguous because in the limit $k_0\downarrow k_\nu^\lambda(\beta_\nu^{\lambda,\min})$ the amplitudes (4.11), (4.20) of the guided modes vanish and hence the function

$$|E^j_{\bar{\kappa}\lambda\nu}(\mathbf{r})|^2|_{\bar{\kappa}=(\beta\cos\varphi,\beta\sin\varphi)}, \tag{6.7}$$

which occurs in the integrand of the inner integral, vanishes also. In particular, when k_0 is increased continuously from a value smaller than $k_\nu^\lambda(\beta_\nu^{\lambda,\min})$ to a value larger than this number, a guided mode is born along the way and an additional term appears in the final sum over guided modes to the right of Eq. (6.6). But since the amplitude of the electric field of a guided mode vanishes at the birth of the mode, the total sum over the guided modes changes continuously with k_0. The integral over the radiation modes to the right of Eq. (6.6) evidently also depends continuously on k_0 and we hence conclude that the zero-point field fluctuations depend continuously on k_0 and in particular that the $\mathcal{F}^j$ do not jump at the birth of a guided mode. In a similar way it follows that the zero-point field fluctuations also depend continuously on the other physical parameters that characterize the system such as the refractive indices and the thickness of the film. The derivative of Eq. (6.7) with respect to these parameters does not vanish, however, at the birth of a guided mode and therefore the derivative of the field fluctuations with respect to these parameters will in general be discontinuous at the birth of a guided mode.

The integral over φ for the three components $j=x,y,z$ in Eq. (6.6) can be computed explicitly. Because the expressions that are obtained are rather complex, we will omit them. The results for the x and y components are identical as they should be.

For the mean of the three components,

$$\mathcal{F}(z)=\tfrac{1}{3}[\mathcal{F}^x(z)+\mathcal{F}^y(z)+\mathcal{F}^z(z)], \tag{6.8}$$

the result of the integral over φ yields a rather concise formula. The quantity $\mathcal{F}(z)$ is the zero-point field fluctuation of a randomly oriented atom at depth z and is therefore of special interest. It is easy to infer from the formulas for the electric fields of the modes in Sec. III and Sec. IV that for $\kappa=(\beta\cos\varphi,\beta\sin\varphi,k_0)$ and $\bar{\kappa}=[\beta_\nu^\lambda(k_0)\cos\varphi,\beta_\nu^\lambda(k_0)\sin\varphi]$ the squared amplitudes

$$|\mathbf{E}_{\kappa\lambda\mu}(\mathbf{r})|^2=\sum_j |E^j_{\kappa\lambda\mu}(\mathbf{r})|^2$$

and

$$|\mathbf{E}^-_{\kappa\lambda\nu}(\mathbf{r})|^2=\sum_j |E^j_{\bar{\kappa}\lambda\nu}(\mathbf{r})|^2$$

are independent of φ. Hence we may take $\varphi=0$ in these sums. It then follows from Eq. (6.6) that

$$\mathcal{F}(z)=\frac{2\pi}{3}\sum_{\lambda=S,P}\sum_{\mu=2}^{3}\int_0^{k_0 n_\mu}\frac{\hbar\omega_0}{2\epsilon_0}|\mathbf{E}_{\kappa\lambda\mu}(\mathbf{r})|^2|_{\kappa=(\beta,0,k_0)}\beta d\beta$$
$$+\frac{2\pi}{3}\sum_{\lambda=S,P}\sum_{\substack{\nu\geqslant 1\\ k_\nu^{\lambda,\min}<k_0}}\frac{\hbar\omega_0}{2\epsilon_0}|\mathbf{E}^-_{\kappa\lambda\nu}(\mathbf{r})|^2|^-_{\kappa=(\beta_\nu^\lambda(k_0),0)}\beta_\nu^\lambda(k_0)\frac{d\beta_\nu^\lambda}{dk}(k_0). \tag{6.9}$$

The remaining integrals with respect to β have to be computed numerically.

Consider now the zero-point field fluctuations in a homogeneous dielectric with a refractive index n_1. By substituting $n_2=n_3=n_1$ into the expressions for the radiation modes listed in Sec. III, we find

$$\mathbf{E}_{\kappa,\lambda,\mu}(\mathbf{r})=\begin{cases} A\exp(i\mathbf{k}_1^+\cdot\mathbf{r})\hat{\mathbf{i}}(\mathbf{k}_1^+,\lambda) & \text{for } \mu=2,\quad \lambda=S,P,\quad \kappa=(k_x,k_y,k), \qquad (6.10a)\\ A\exp(i\mathbf{k}_1^-\cdot\mathbf{r})\hat{\mathbf{i}}(\mathbf{k}_1^-,\lambda) & \text{for } \mu=3,\quad \lambda=S,P,\quad \kappa=(k_x,k_y,k), \qquad (6.10b)\end{cases}$$

where $(k_x^2+k_y^2)^{1/2}<kn_1$ and where

$$A=\frac{1}{(2\pi)^{3/2}}\left(\frac{k}{k_{1z}}\right)^{1/2} \tag{6.11}$$

to ensure that the modes are orthonormal. Hence the radiation modes reduce to plane waves. In a homogeneous space guided modes obviously do not exist. By substituting Eqs. (6.10a), (6.10b), and (6.11) into Eq. (6.6) we find for the components of the zero-point field fluctuations in a homogeneous dielectric of refractive index n_1:

$$\mathcal{F}^x=\mathcal{F}^y=\mathcal{F}^z=n_1\mathcal{F}_{\text{free}}, \tag{6.12}$$

where $\mathcal{F}_{\text{free}}$ denotes the vacuum field fluctuations (in free space):

$$\mathcal{F}_{\text{free}}=\frac{\hbar\omega_0^3}{6\pi^2\epsilon_0 c^2}. \tag{6.13}$$

For an atom at depth z inside the slab having a dipole moment parallel to the jth coordinate axis the spontaneous emission rate relative to the value in vacuum is

$$\mathcal{F}^j(z)/\mathcal{F}_{\text{free}}, \tag{6.14}$$

while for a randomly oriented atom the relative transition rate is

$$\mathcal{F}(z)/\mathcal{F}_{\text{free}}, \tag{6.15}$$

with $\mathcal{F}(z)$ being defined by Eq. (6.8). In the following the symbols $\mathcal{F}^j$ and $\mathcal{F}$ will always refer to spontaneous emission rates relative to the free-space value as defined by Eqs. (6.14) and (6.15), respectively.

Finally, the mean relative spontaneous emission rate relative to free space of the total film is obtained by computing the mean of Eq. (6.15) over the thickness of the film.

VII. POSITION DEPENDENCE OF THE ZERO-POINT FIELD FLUCTUATIONS

In this section we will briefly consider the z dependence of the zero-point field fluctuations (relative to the value in free space). We will compare our results with those published previously in [18] and will therefore restrict the examples to symmetric slab waveguides.

The refractive index of the two half spaces is taken equal to 1. In Figs. 4 and 5 the x and z components of the zero-point field fluctuations are shown as functions of $2z/d$ for three choices of the refractive index of the slab, namely, $n_1=4.0$, $n_1=2.0$, and $n_1=1.5$. The thickness of the slab is $d=0.1\lambda_0$, where λ_0 is the emission wavelength. For all three choices of n_1 there is one guided S-polarized and one guided P-polarized mode. As follows from Eq. (6.6), the zero-point field fluctuations consist of two separate contributions, namely, that of the radiation modes and that of the guided modes. These contributions are also shown in Figs. 4 and 5. It is seen that $\mathcal{F}^x(z)$ and $\mathcal{F}^z(z)$ approach the bulk value in free space at large distances from the slab.

A second example is shown in Figs. 6 and 7. This case

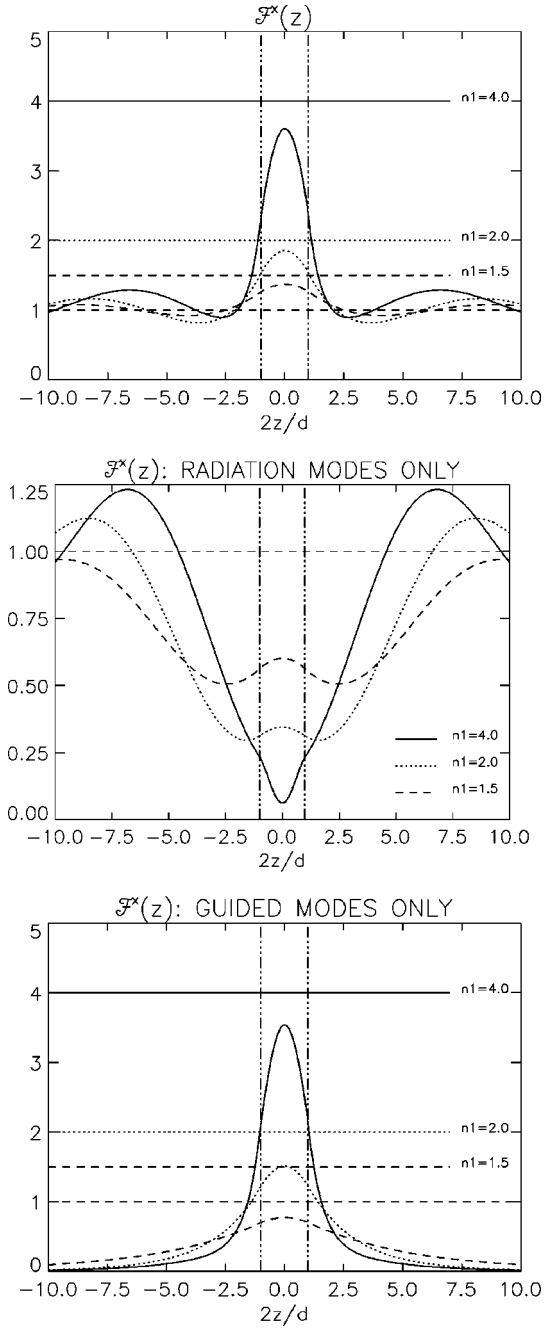

FIG. 4. X component of the zero-point field fluctuations $\mathcal{F}(z)$ (relative to the value in free space) as a function of $2z/d$ and the contribution of the radiation and the guided modes to $\mathcal{F}^x(z)$ for three refractive indices of the slab. The refractive index of the half spaces $|z|>d/2$ is 1 and the thickness of the slab is 0.1 times the emission wavelength.

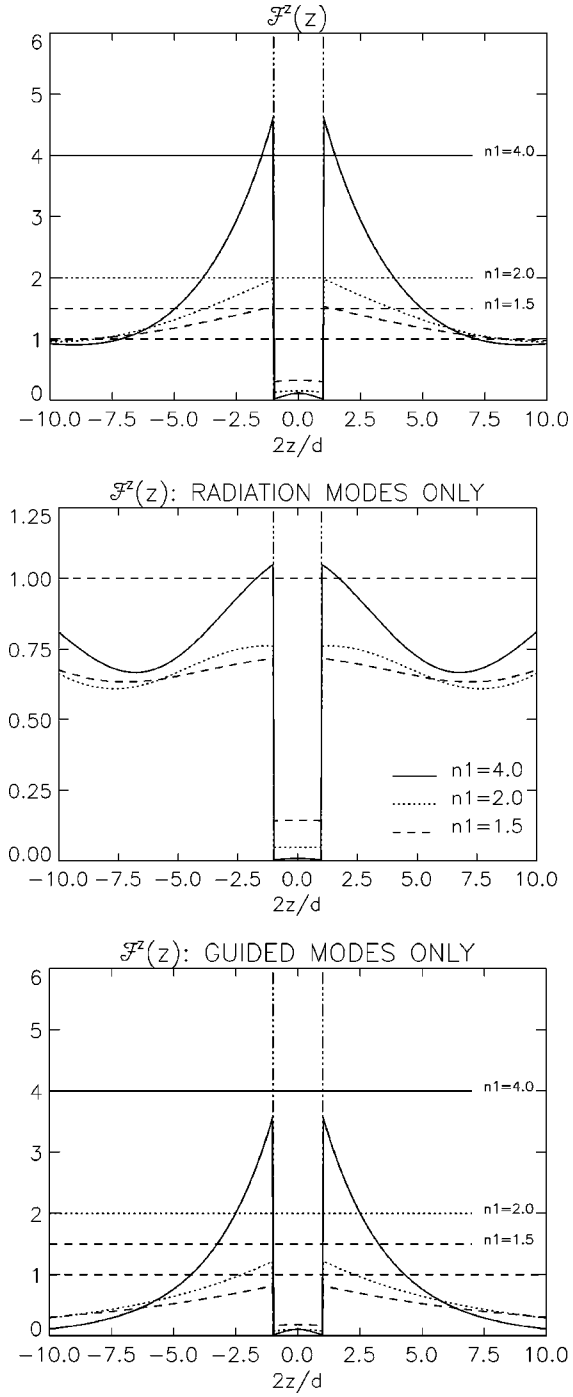

FIG. 5. Z component of the zero-point field fluctuations $\mathcal{F}(z)$ as a function of $2z/d$ and the contribution of the radiation and the guided modes to $\mathcal{F}^z(z)$ for three refractive indices of the slab. The refractive index of the half spaces $|z|>d/2$ is 1 and the thickness of the slab is 0.1 times the emission wavelength.

differs from the previous one only in the thickness of the slab, which is now equal to the emission wavelength: $d=\lambda_0$. For $n_1=1.5$ there are now three S- and three P-polarized guided modes, i.e., $M_S=M_P=3$. For $n_1=2.0$ $M_S=M_P=4$ and for $n_1=4.0$ $M_S=M_P=8$. In all cases the contribution of the radiation modes to the zero-point field fluctuations inside the slab is considerably smaller than the contribution of the guided modes. Furthermore, near the middle of the slab, $\mathcal{F}^x(z)$ and $\mathcal{F}^z(z)$ are almost equal to the bulk value.

Comparison of these figures with the corresponding ones in [18] shows that the zero-point field fluctuations pertaining to the radiation modes agree with our results, but that the contributions of the guided modes differ. The z component of the field fluctuations is discontinuous at the surfaces of the slab due to the discontinuity of the z components of the electric fields of the modes (ϵE_z is continuous). However, the jump that we find is much smaller than in [18]. The differences are caused by the fact that the density of the guided modes as computed in Eq. (4.13) of [18] is not cor-

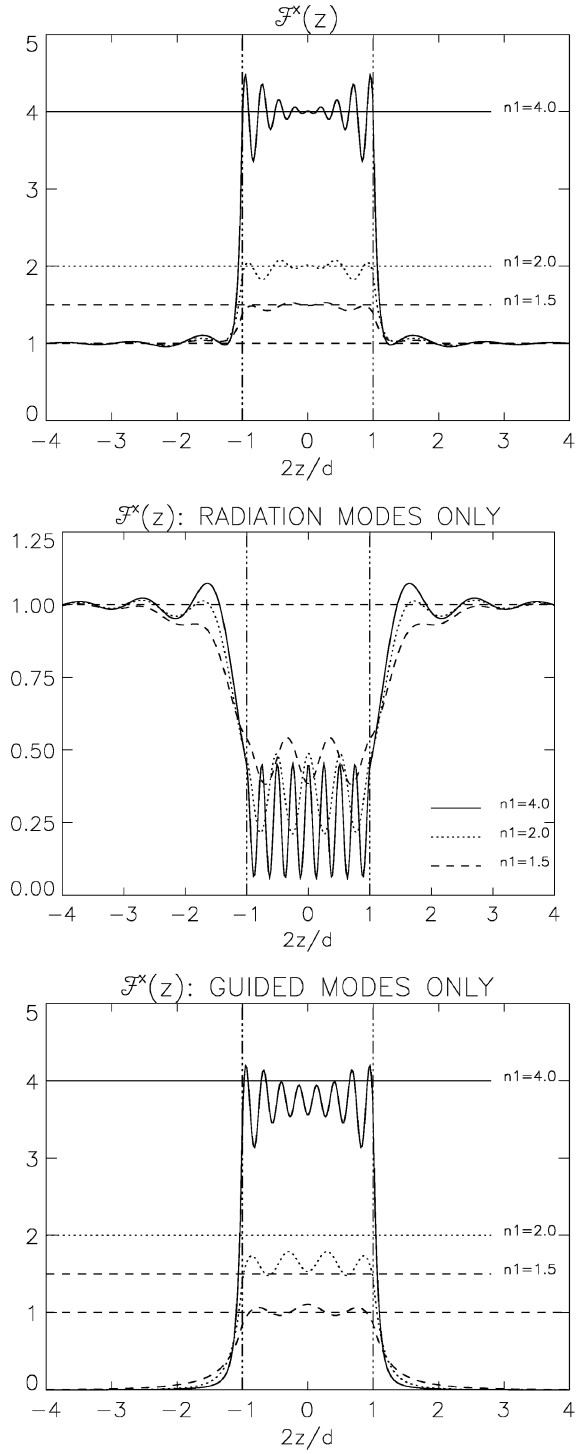

FIG. 6. X component of the zero-point field fluctuations $\mathcal{F}(z)$ as a function of $2z/d$ and the contribution of the radiation and the guided modes to $\mathcal{F}^x(z)$ for three refractive indices of the slab. The refractive index of the half spaces $|z|>d/2$ is 1 and the thickness of the slab is equal to the emission wavelength.

rect because the factor $d\beta_\nu^\lambda/dk$ to the right of Eq. (6.9) is missing. Furthermore, Eqs. (2.12) and (2.15) of [18] that correspond to the P-polarized guided symmetric and antisymmetric modes are erroneous.

In the examples just mentioned, the refractive index in the film is larger than in the half spaces. In Fig. 8 the reverse case is shown. The refractive index in the half spaces is 2.0 whereas in the slab it is 1.8, 1.5, and 1.0, respectively. The thickness of the slab is $d=0.1\lambda_0$. In this case there are of course no guided modes, so only the radiation modes contribute. Because the refractive index in the slab is lower than in the half spaces, the z component of the electric fields of the modes is larger on the side of the slab of the interface than on the side of the half space. Therefore, the same holds for $\mathcal{F}^z(z)$. On the other hand, $\mathcal{F}^x(z)$ is continuous and smoothly varying. Figure 9 is analogous to Fig. 8 but with $d=\lambda_0$. The jumps of $\mathcal{F}^z(z)$ at the interfaces are as expected and $\mathcal{F}^x(z)$ is smooth. At this thickness the value of the zero-point field fluctuations in the middle of the slab is again very close to the bulk value.

VIII. COMPARISON WITH EXPERIMENTAL RESULTS

We will first apply the model to a configuration of an experiment discussed by Yablonovitch *et al.* [15]. It concerns the spontaneous emission of light from electron-hole recombination in thin GaAs slabs. The GaAs film is transferred onto several substrates with air or vacuum above the film and the emission rate is measured as a function of the refractive index n of the substrate. The refractive index of GaAs at the emission wavelength is 3.6.

The emission rate of the film is computed by taking the mean over the film thickness of the zero-point field fluctuations $\mathcal{F}(z)$ (relative to vacuum). At the left of Fig. 10 the computed mean $\mathcal{F}$ of the film is shown as a function of n for two films of thicknesses 0.25λ and 3λ when all modes are taken into account in the calculation and when only the radiation modes contribute. It was stated in [15] that guided modes do not contribute to the measured spontaneous emission rate due to reabsorption in the film. It is seen in the figure that when all modes are taken into account the emission rate is a slowly increasing function of n. For the thicker film the mean $\mathcal{F}$ is almost constant and equal to the bulk value 3.6. Hence in this case the influence of the half spaces is negligible. When the guided modes are disregarded, the computations yield more steeply increasing functions. The wiggles in the curves correspond to the disappearance of guided modes. At $n=1$ there are two guided modes of either polarization for the thinner film and twenty of either polarization for the thicker film. When n is larger than the refractive index 3.6 of GaAs there are no guided modes and hence the curves with and without guided modes then coincide.

Yablonovitch *et al.* postulated that for films thinner than half the emission wavelength the emission rate will be proportional to n whereas for films whose thickness is several wavelengths the emission rate will be proportional to n^2+1. To verify this the functions $\mathcal{F}/n$ and $\mathcal{F}/(n^2+1)$ are shown at the right of Fig. 10 for the thin and the thicker film, respectively (here $\mathcal{F}$ is again the mean emission rate of the film). It is seen that for the thinner film the calculations do not confirm the hypothesis but that for the thicker film $\mathcal{F}/(n^2+1)$ is indeed approximately constant when the guided modes are disregarded in the calculations.

Next we will consider the change of the spontaneous emission of Eu^{3+} ions in a thin film when the surrounding of the ions is changed. In [16] the spontaneous emission was measured of a complex of an Eu^{3+} ion with three hexafluoroacetylacetonate ligands and two tri-octylphosphine oxide

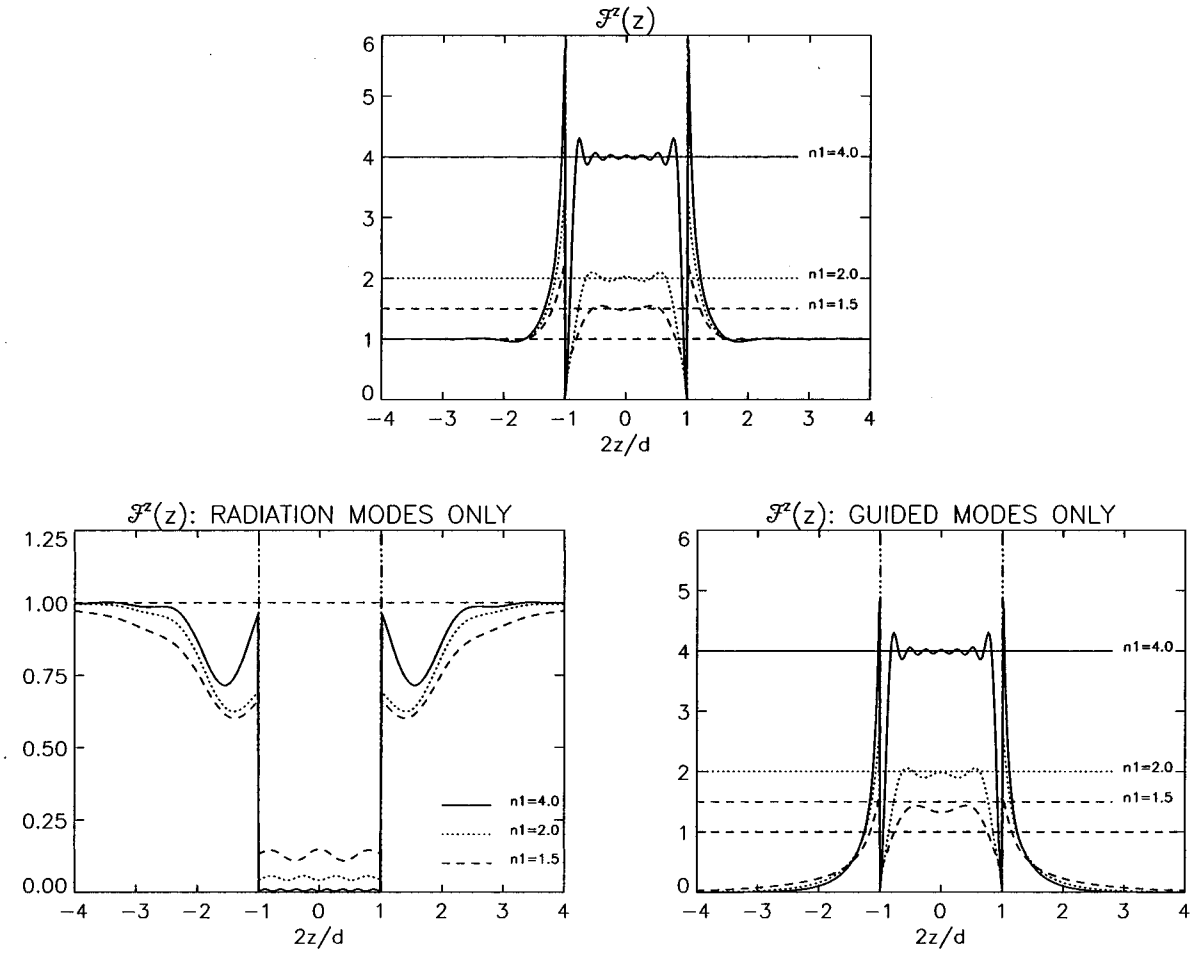

FIG. 7. Z component of the zero-point field fluctuations $\mathcal{F}(z)$ as a function of $2z/d$ and the contribution of the radiation and the guided modes to $\mathcal{F}^z(z)$ for three refractive indices of the slab. The refractive index of the half spaces $|z|>d/2$ is 1 and the thickness of the slab is equal to the emission wavelength.

molecules as synergistic agends (Eu^{3+}-hfa-topo) [17]. The ligand can be optically excited around 300 nm, after which the energy is transferred to the Eu^{3+} ion in the $^5D_0$ level, followed by radiative decay to the ^7F_i levels, $i=0,\ldots,6$ at a wavelength of 611 nm. The $^5D_0$ lifetime of the Eu^{3+} hfa-topo complex is almost completely determined by electric dipole transitions.

Thin films of $0.01M$ Eu^{3+} hfa-topo in polystyrene (PS) of various thicknesses were spin-coated onto several substrates with surfaces polished to an optical quality. The thickness variations in a given film were less than 5%. The refractive index of the PS films at the wavelength of emission of 611 nm was 1.585 and absorption was negligible at this wavelength.

The mean emission rate of a PS film relative to the bulk value is found by calculating the mean over the film thickness of the function $\mathcal{F}(z)/n_1$, where n_1 is the refractive index of the film at the emission wavelength and $\mathcal{F}(z)$ is the transition rate of a randomly oriented atom at a depth z relative to free space. By multiplying this mean rate by the emission rate $1/\tau_{\text{bulk}}=1.531$ msec^{-1} measured in bulk PS, we obtain the film's emission rate in msec^{-1}.

The purpose of the first experiment for the Eu^{3+} complexes that we will discuss was to verify the computed emission rate in a thin film adjacent to an interface between two media with different refractive indices. Because the emission rate in such a film depends on the zero-point field fluctuations close to the interface, this experiment indirectly verifies the computed field fluctuations close to an interface. A 70-nm-thick PS film containing the Eu^{3+} hfa-topo complex was intermediate between a thick glass substrate and a ZnSe layer. The refractive indices of the PS film and of the glass substrate are both 1.585 at the fluorescence wavelength of $\lambda_0=611$ nm. The ZnSe layer has refractive index 2.61. Above the ZnSe layer there was either air (asymmetric configuration) or a 1-μm-thick glass layer (symmetric configuration, see Fig. 11). Because the glass and the PS film have the same refractive index the configuration consists optically of three different media. In Fig. 12 measured and computed emission rates are shown as a function of the thickness of the ZnSe layer. Computed emission rates obtained by neglecting the guided modes are also shown. The most left measured data in Fig. 12 correspond to the case where the ZnSe layer is absent (thickness is zero). The emission rate in the symmetric configuration is then approximately equal to the bulk value of 1.531 msec^{-1}. For both configurations the emission rate of the PS film is an oscillating function of the thickness of the ZnSe layer. At large thicknesses it becomes equal to 1.988 msec^{-1}, which is the emission rate of a 70-nm-thick fluorescence film adjacent to the interface between two half

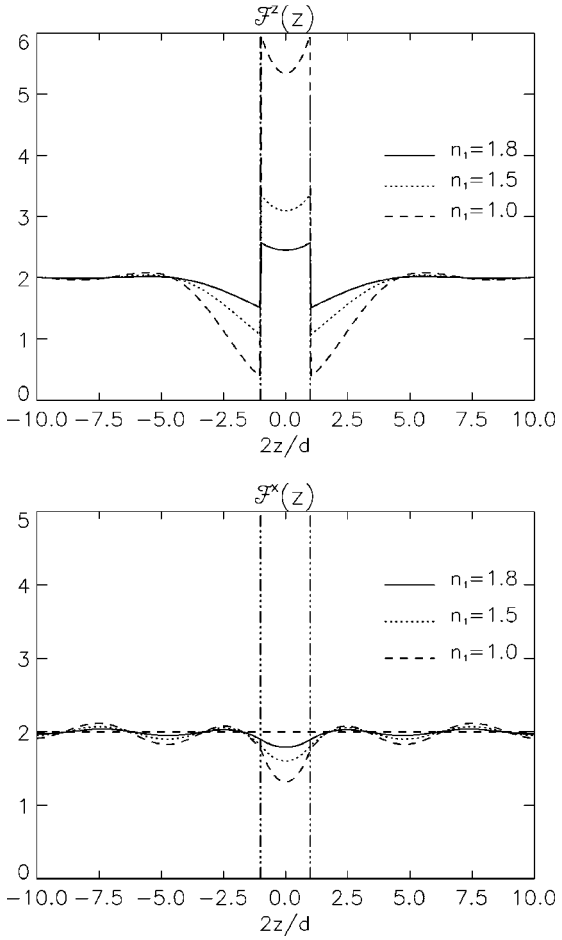

FIG. 8. X and z components of the zero-point field fluctuations $\mathcal{F}(z)$ as functions of $2z/d$ for a slab for three refractive indices of the slab that are lower than the refractive index $n_2=2$ of the half spaces $|z|>d/2$. The thickness of the slab is equal to 0.1 times the emission wavelength.

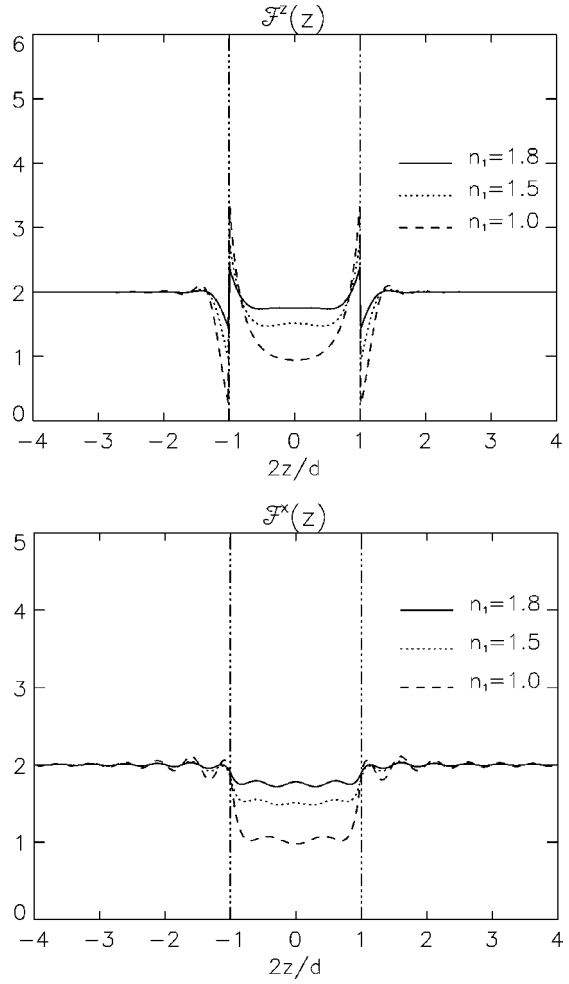

FIG. 9. Same as Fig. 8 but now for a slab thickness equal to the emission wavelength.

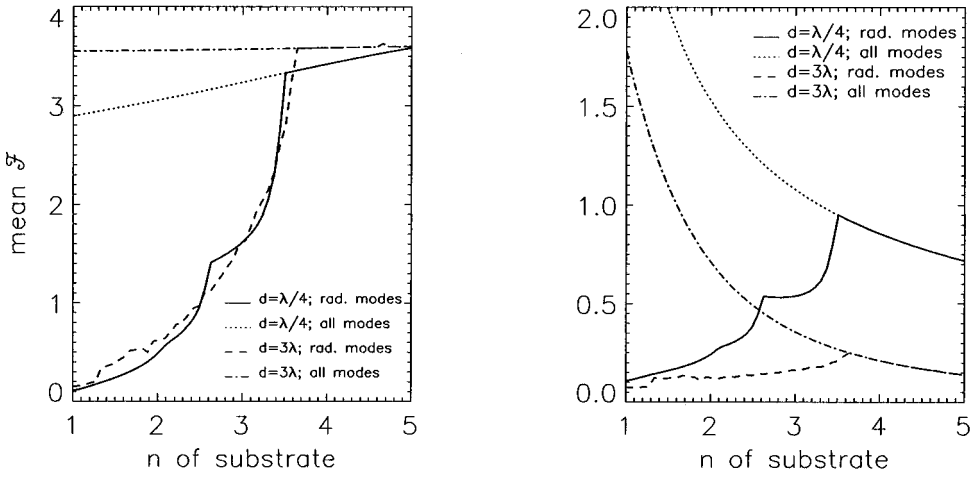

FIG. 10. Mean zero-point field fluctuations of GaAs films bounded by air and by a substrate of varying refractive index. The thicknesses of the film are 0.25λ and 3λ, with λ the emission wavelength. The refractive index of GaAs is 3.6. In the left figure the mean $\mathcal{F}$ is shown as a function of the refractive index of the substrate when only radiation modes are taken into account and when all modes are assumed to contribute. In the right figure, $\mathcal{F}/n$ is shown as a function of n for the film of thickness λ/4 and $\mathcal{F}/(n^2+1)$ is shown for the film of thickness 3λ.

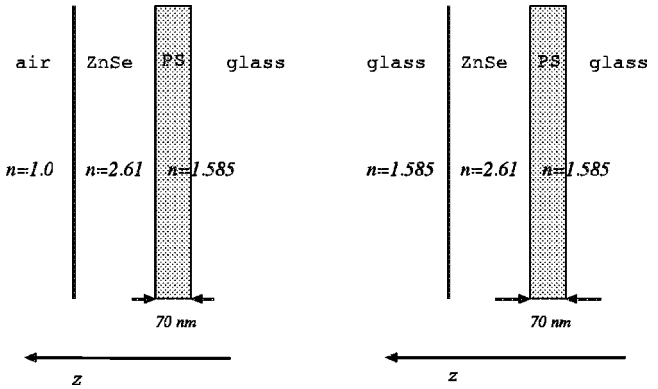

FIG. 11. Asymmetric (left) and symmetric (right) configurations of the experiments of Fig. 12. A 70-nm-thick PS film doped by $0.01M$ Eu^{3+} hfa-topo is intermediate between a thick glass substrate with the same refractive index 1.585 as the PS film and a ZnSe layer with refractive index 2.61. In the asymmetrical configuration there is air above the ZnSe layer whereas in the symmetrical configuration the ZnSe layer is covered by a thick glass layer.

spaces filled with glass and ZnSe, respectively, with the PS film on the side of the glass. It is seen that measured and computed rates agree reasonably well for the smallest three layer thicknesses. The calculations in [18] show a much stronger dependence of the spontaneous emission rate on the thickness of the ZnSe layer due to the incorrect computation of the contribution of the guided modes mentioned above.

It is seen in Fig. 12 that when only the contribution of the radiation modes is taken into account, computed emission rates differ considerably from the rates that include the contribution of the guided modes and from measured emission rates. Hence, the contribution of the guided modes to the zero-point field fluctuations and hence also to the spontaneous emission rates is significant. At all thicknesses of the ZnSe layer in the symmetric configuration and at thicknesses larger than 35 nm in the asymmetric case there are guided modes. For a thickness of 550 nm we have $M_S = M_P = 4$ in both configurations. Because of the significant contribution of the guided modes, the experiment of Fig. 12 verifies indirectly the calculated contribution of the guided modes to the zero-point field fluctuations.

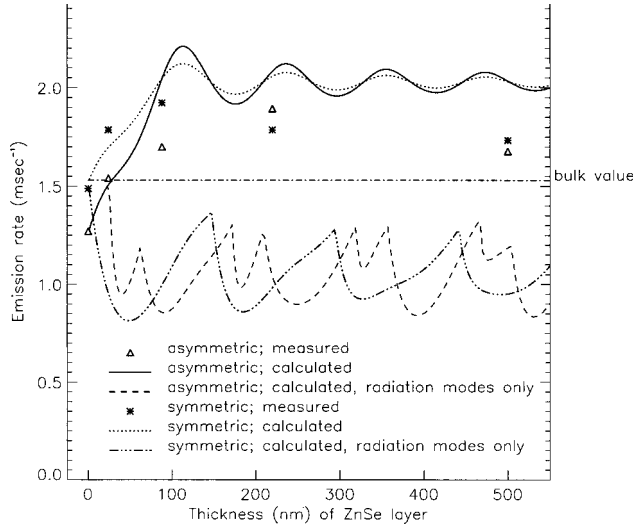

FIG. 12. Measured and computed emission rates of $0.01M$ Eu^{3+} hfa-topo complex in a 70-nm-thick PS film for the symmetric and asymmetric configurations shown in Fig. 11. The emission rate is shown as a function of the thickness of the ZnSe layer. The emission wavelength is 611 nm. The refractive index of the film and the substrate are both 1.585 and the refractive index of the ZnSe layer is 2.61. The emission rate in bulk is 1.531 $msec^{-1}$. The continuous and dotted curves are the calculated emission rates for the asymmetric and the symmetric configuration, respectively. In addition, the dashed and dashed-dotted curves are the rates that are obtained when the contribution of the guided modes to the zero-point field fluctuations are neglected.

TABLE I. Real and imaginary parts n and κ of the refractive indices of the substrates at 611 nm. LF5 and SF59 are manufactured by Schott Glaswerke.

Substrate	n	κ
LiF	1.385	0
Fused quartz	1.465	0
Soda lime glass	1.51	0
LF5 glass	1.585	0
MgO	1.735	0
SF59 glass	1.945	0
$SrTiO_3$	2.44	0
ZnSe	2.61	4×10^{-6}
As_2Se_3	3.2	0.11
GaP	3.34	$<1\times10^{-5}$
Si	3.92	0.024
Ge	5.64	1.04

At larger thicknesses of the ZnSe layer, differences between measured and computed emission rates are bigger. This is probably due to the absorption of radiation in this layer. Our model cannot account for absorption. According to Table I the imaginary part of the refractive index of the ZnSe layer at the fluorescence wavelength is not negligible. It is well known both theoretically [27] and experimentally [9,28], that a radiating atom in the neighborhood of a medium with a complex refractive index suffers significantly from non-radiative decay. Hence the spontaneous emission rate in the film is decreased and this effect is likely to be more profound at larger thicknesses of the ZnSe layer.

Next we consider the mean spontaneous emission rate of Eu^{3+} hfa-topo doped PS films as a function of film thickness. Figure 13 shows measured and computed rates for films on fused quartz substrates having a refractive index of 1.465 at 611 nm and negligible absorption. Good agreement between computed and measured emission rates is observed at thicknesses $\geqslant 30$ nm. At thicknesses larger than 1 μm ($n_{PS}d/\lambda_0 = 2.58$), the measured and computed rates are almost equal to the bulk value of 1.531 $msec^{-1}$.

The marked points on the continuous curve in Fig. 13 refer to thicknesses at which the number of guided modes changes. There are no guided modes for thicknesses smaller than 0.15 μm. Hence the main increase in the emission rate in Fig. 14 occurs at thicknesses at which there are only radiation modes in the structure. The number of guided modes increases with d from $M_S = 1$, $M_P = 0$ at $d = 0.215$ μm to $M_S = M_P = 20$ at $d = 10$ μm. In Fig. 14 the zero-point field fluctuations (with respect to the free space value) are shown as a function of z at film thickness $d = 20$ nm, $d = 150$ nm, and $d = 500$ nm. There are no guided modes for the lowest

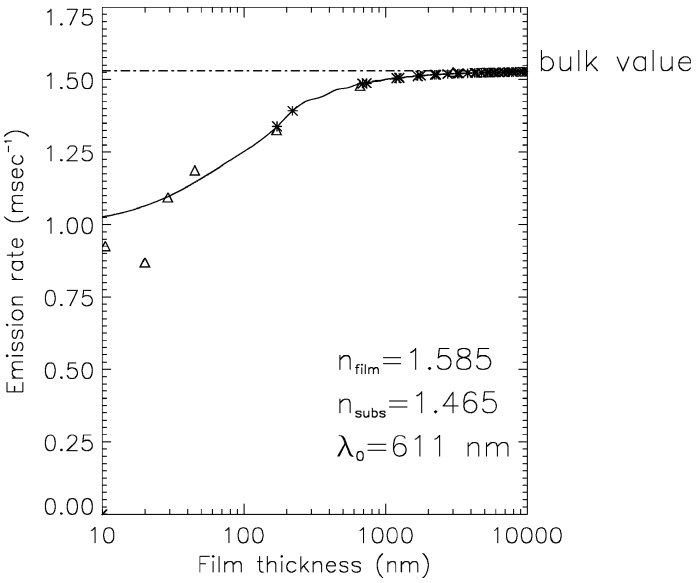

FIG. 13. Measured and computed emission rates of $0.01M$ Eu^{3+} hfa-topo complex in PS films on fused quartz substrates as a function of the film thickness. The measurements are indicated by triangles. The asterisks on the curve correspond to thicknesses at which the number of guided modes changes. The emission wavelength is 611 nm, the refractive indices of the film and the substrate are 1.585 and 1.465, respectively. The emission rate in bulk is 1.531 $msec^{-1}$.

two thicknesses, while for $d=500$ nm we have $M_S=M_P=1$. It is seen that the jump of the refractive index at the surface of the PS film causes a jump of the zero-point field fluctuations from a relatively low value on the side of the PS film to a relatively large value on the side of the vacuum. In the case of thicker films the influence of the jump is small and the emission rate of the film approaches the bulk value.

Next we will consider the influence of the refractive index of the substrate on the emission rate of the film. Figure 15 shows measured and computed rates of three Eu^{3+} hfa-topo doped PS films with thicknesses $d=660$ nm, $d=170$ nm, and $d=45$ nm, for several substrates listed in Table I. The curves in Fig. 15 were obtained by computations. At substrate refractive indices larger than the refractive index of the film ($n_{PS}=1.585$), the zero-point field fluctuations in the film and near the substrate are relatively large. Therefore, the emission rate of the film is larger than the bulk value, especially with thinner films. On the other hand, when the refractive index of the substrate is smaller than the refractive index of the film, the reverse occurs. Due to the jump in the z component of the electric fields of the modes, $\mathcal{F}(z)$ is relatively small near the substrate in the film and this causes a smaller emission rate. Again the effects are the strongest with the thinnest films and therefore the curves in Fig. 15 cross.

In Fig. 16, $\mathcal{F}(z)$ is shown for a 170-nm-thick film and for three substrate indices: $n_2=1.385$, $n_2=1.585$, and $n_2=3.92$, corresponding to LiF, LF5 glass, and Si, respectively (see Table I). These figures clearly illustrate the influence of the jump at the interface between the film and the substrate on the zero-point field fluctuations.

In the case of a thickness of 660 nm ($n_{PS}d/\lambda_0=1.71$), the influence of the substrate on the lifetime is small and the

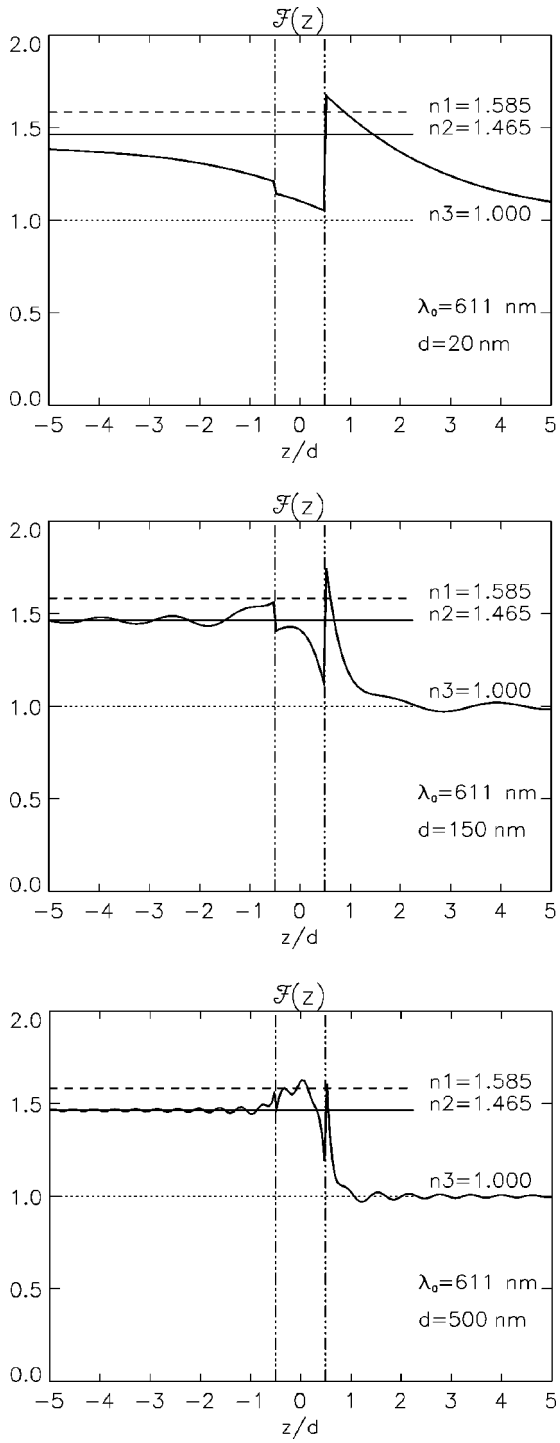

FIG. 14. The zero-point field fluctuations $\mathcal{F}(z)$ as functions of z/d for the Eu^{3+} hfa-topo complex in PS films with a refractive index of 1.585 at 611 nm on a fused quartz substrate ($z<-d/2$) having a refractive index of 1.465. The thickness of the film is $d=20$ nm in the upper figure, 150 nm in the middle figure, and 500 nm in the lower figure.

emission rate differs little from the bulk value. The measured and computed rates of all three films agree well for the lower substrate indices. However, the lowest substrate index corresponding to LiF is an exception. It was postulated in [16] that the measured rather steep decrease in the emission rate at the lowest refractive index is caused by the contribution of the guided modes, which are only present in the case of the

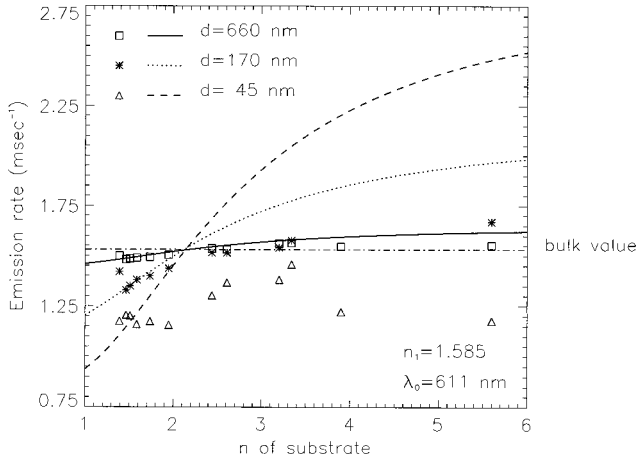

FIG. 15. Measured and computed emission rates of the Eu^{3+} hfa-topo complex in PS films as functions of the refractive index of the substrate for three different film thicknesses: 660 nm, 170 nm, and 45 nm. The emission wavelength is 611 nm.

lowest refractive indices (see Table II). But the computations predict a monotonically smoothly increasing mean $\mathcal{F}$ for increasing refractive indices.

The measurements and computations show poor agreement for larger substrate indices, especially for the 45-nm-thick film. This is due to the fact that these substrates absorb radiation at a wavelength of 611 nm. The high absorption of some of the substrates with relatively high refractive index can reduce the mean spontaneous emission rate of the film in spite of the fact that the high refractive index tends to increase the photon density of states in the film. To verify this quantitatively a more sophisticated model is needed in which the absorption is incorporated on a microscopic level as suggested by Hopfield [21]. In particular, an extension of Yeung's analysis [24] to the case of a slab geometry would be needed.

IX. CONCLUSION

We have calculated the spontaneous emission rate of emitters located in a nonabsorbing dielectric structure consisting of a slab, bounded on both sides by infinite half spaces of arbitrary, real refractive indices. We have compared our results with earlier calculations, correcting some mistakes, and with experimental results, finding fair agreement.

TABLE II. The pairs (M_S, M_P) of the number of guided S-polarized and P-polarized modes for the different substrates mentioned in Table I and for three film thicknesses. The substrates that are not explicitly mentioned have refractive indices larger than index of the film, which means that no guided modes exist.

Substrate, n_{subsrate}	$d=45$ nm	$d=170$ nm	$d=660$ nm
LiF, $n=1.385$	(0,0)	(1,1)	(2,2)
Fused quartz, $n=1.465$	(0,0)	(1,0)	(1,1)
Soda lime glass, $n=1.510$	(0,0)	(0,0)	(0,0)
$n \geqslant 1.585$	(0,0)	(0,0)	(0,0)

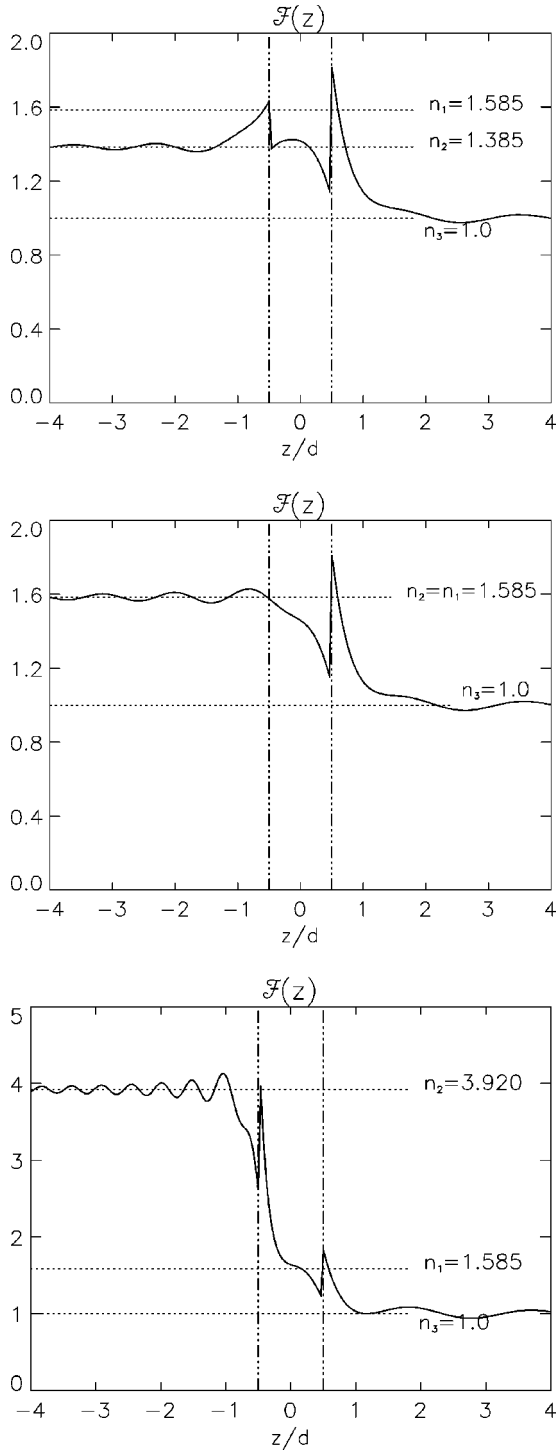

FIG. 16. The zero-point field fluctuations $\mathcal{F}(z)$ as functions of z/d for the Eu^{3+} hfa-topo complex in a PS film with a thickness of 170 nm and with a refractive index of 1.585 on three different substrates. The refractive indices of the substrates are from top to bottom 1.385, 1.585 (matched substrate), and 3.92.

APPENDIX A: SOME NUMERICAL CONSIDERATIONS

The integrals over the radiation modes in expression (6.6) for the components $\mathcal{F}^j(z)$ of the zero-point field fluctuations have to be computed numerically. We will consider the integral for $j=x$, $\lambda=S$, and $\mu=2$ in some more detail. By substituting field amplitudes (3.2a), (3.2b), (3.2c), and (3.7) into Eq. (6.6), one finds after computing the integral over φ:

$$\frac{1}{8\pi^2}\frac{\hbar\omega_0}{2\epsilon_0}\int_0^{k_0 n_2}|T\ \exp(i\mathbf{k}_{3z}z)|^2\frac{k_0}{k_{2z}}\beta d\beta \quad \text{for } z\geqslant d/2, \tag{A1}$$

$$\frac{1}{8\pi^2}\frac{\hbar\omega_0}{2\epsilon_0}\int_0^{k_0 n_2}|U\ \exp(i\mathbf{k}_{1z}z)+V\ \exp(-i\mathbf{k}_{1z}z)|^2\frac{k_0}{k_{2z}}\beta d\beta$$

$$\text{for } -d/2\leqslant z\leqslant d/2, \tag{A2}$$

$$\frac{1}{8\pi^2}\frac{\hbar\omega_0}{2\epsilon_0}\int_0^{k_0 n_2}|\exp(i\mathbf{k}_{2z}z)+R\ \exp(-i\mathbf{k}_{2z}z)|^2\frac{k_0}{k_{2z}}\beta d\beta$$

$$\text{for } z\leqslant -d/2, \tag{A3}$$

with U, V, T, and R being given by Eqs. (3.3), (3.4), (3.5), and (3.6). To compute these and similar integrals fast and accurately, singularities in the integrands should be eliminated by changing the integration variable. Not only have the integrands above a square root singularity at $\beta=k_0n_2$ due to the occurrence of k_{2z} in the numerator, but the derivative of the integrand with respect to β moreover has singularities at $\beta=k_0n_1$ and at $\beta=k_0n_3$ due to the presence of k_{1z} and k_{3z} in U, V, R, and T and in the exponentials. The integrals over $(0,k_0n_2)$ are therefore written as a sum of integrals over intervals having exactly one of k_0n_1, k_0n_2, or k_0n_3 as an endpoint. In each of these intervals the integrand is made smooth by a transformation of integration variable that eliminates the square root causing the singularity. The numerical integration is then carried out using the Romberg integration method. For smooth (i.e., infinitely differentiable) integrands, this method converges very fast because at every new iteration the order of convergence increases by 1. After specifying a desired accuracy, the method will perform as many iterations as is required to achieve this accuracy. This is important because with certain configurations, the integrands can be highly oscillatory and therefore choosing a fixed grid beforehand is risky.

It should be noted that the factor

$$1-r_{12}r_{13}\exp(2ik_{1z}d) \tag{A4}$$

occurs in the numerator of U, V, R, and T. In the S-polarized case this factor vanishes when

$$\frac{(k_{1z}-k_{3z})(k_{1z}-k_{2z})}{(k_{1z}+k_{3z})(k_{1z}+k_{2z})}=\exp(-2ik_{1z}d). \tag{A5}$$

This happens when $k_{1z}=0$. It may also happen when $k_{1z}>0$, namely, when an S-polarized guided mode is born. In fact, Eq. (A5) is identical to Eq. (4.3) that is satisfied by the propagation constant of an S-polarized guided mode. Whenever Eq. (A4) vanishes, the integrands in Eqs. (A1), (A2), and (A3) have to be replaced by their finite limits.

[1] E. M. Purcell, Phys. Rev. **69**, 681 (1946).
[2] R. G. Hulet, E. S. Hilfer, and D. Kleppner, Phys. Rev. Lett. **55**, 2137 (1985).
[3] W. Jhe, A. Anderson, E. A. Hinds, D. Meschede, L. Moi, and S. Haroche, Phys. Rev. Lett. **58**, 1320 (1987).
[4] D. J. Heinzen and M. S. Feld, Phys. Rev. Lett. **59**, 2623 (1987).
[5] F. de Martini, G. Innocenti, G. R. Jacopbovitz, and P. Mataloni, Phys. Rev. Lett. **59**, 2955 (1987).
[6] F. de Martini, M. Marrocco, P. Mataloni, L. Crescentini, and R. Loudon, Phys. Rev. A **43**, 2480 (1991).
[7] Y. Yamamoto, S. Machida, Y. Horikoshi, K. Igeta, and G. Björk, Opt. Commun. **80**, 337 (1991).
[8] A. M. Vredenberg, N. E. J. Hung, E. F. Schubert, D. C. Jacobson, J. M. Poate, and G. J. Zydzik, Phys. Rev. Lett. **71**, 517 (1993).
[9] K. H. Drexhage, J. Lumin. **1–2**, 693 (1970).
[10] C. K. Carniglia, L. Mandel, and K. H. Drexhage, J. Opt. Soc. Am. **62**, 479 (1972).
[11] K. H. Drexhage, in *Progress in Optics*, edited by E. Wolf (North-Holland, Amsterdam, 1974), Vol. XII.
[12] C. K. Carniglia and L. Mandel, Phys. Rev. D **3**, 280 (1971).
[13] H. Khosravi and R. Loudon, Proc. R. Soc. London, Ser. A **433**, 337 (1991).
[14] E. Snoeks, A. Lagendijk, and A. Polman, Phys. Rev. Lett. **74**, 2459 (1995).
[15] E. Yablonovitch, T. J. Gmitter, and R. Bhat, Phys. Rev. Lett. **61**, 2546 (1988).
[16] G. L. J. A. Rikken, Phys. Rev. A **51**, 4906 (1995).
[17] F. Halverston, J. S. Brinnen, and J. R. Leto, J. Chem. Phys. **41**, 157 (1964).
[18] D. Marcuse, *Theory of Dielectric Optical Waveguides* (Academic Press, New York, 1974).
[19] H. Khosravi and R. Loudon, Proc. R. Soc. London, Ser. A **436**, 373 (1992).
[20] G. L. J. A. Rikken and Y. A. R. R. Kessener, Phys. Rev. Lett. **74**, 880 (1995).
[21] J. J. Hopfield, Phys. Rev. **112**, 1555 (1958).
[22] B. Huttner and S. M. Barnett, Phys. Rev. A **46**, 4306 (1992).
[23] B. Huttner, S. M. Barnett, and R. Loudon, Phys. Rev. Lett. **68**, 3698 (1992).
[24] M. S. Yeung and T. K. Gustafson, Phys. Rev. A **54**, 5227 (1996).
[25] R. Weder, *Spectral and Scattering Theory for Wave Propagation in Perturbed Stratified Media* (Springer-Verlag, New York, 1991).
[26] R. Loudon, *The Quantum Theory of Light* (Clarendon Press, Oxford, 1983), 2nd ed.
[27] B. N. J. Persson, J. Phys. C **11**, 4251 (1978).
[28] G. Cnossen, K. Drabe, and D. Wiersma, J. Chem. Phys. **98**, 5276 (1993).